Radiolabeled selective MMP-13 inhibitors:

(Radio)syntheses, *in vitro* and first *in vivo* evaluations

Verena Hugenberg[a,b,†*], *Stefan Wagner*[b], *Klaus Kopka*[b,††], *Michael Schäfers*[a,b,d], *Robert C. Schuit*[c], *Albert D. Windhorst*[c], *Sven Hermann*[a,d]

[a] European Institute for Molecular Imaging, University of Münster, Waldeyerstr. 15, D-48149 Münster, Germany,

[b] Department of Nuclear Medicine, University Hospital Münster, Albert-Schweitzer-Campus 1, Building A1, D-48149 Münster, Germany,

[c] Department of Radiology & Nuclear Medicine, VU University Medical Center Amsterdam, De Boelelaan 1117, 1081 HZ Amsterdam, The Netherlands,

[d] DFG EXC 1003 Cluster of Excellence 'Cells in Motion', University of Münster, D-48149 Münster, Germany

[†]New address: Institute for Radiology, Nuclear Medicine and Molecular Imaging, Heart and Diabetes Center North Rhine Westphalia, University Hospital, Ruhr University Bochum, Georgstr. 11, D-32545 Bad Oeynhausen, Germany

[††]New address: German Cancer Research Center (dkfz), Division of Radiopharmaceutical Chemistry, Im Neuenheimer Feld 280, D-69120 Heidelberg, Germany.

RECEIVED DATE: September 1, 2016

TITLE RUNNING HEAD. Radiolabeled selective MMP-13 inhibitors: Radiosyntheses, *in vitro* and first *in vivo* evaluation

* to whom correspondence should be addressed. Phone: +495731973551. Fax: +495731971819. E-mail: verena.hugenberg@gmx.de

ABSTRACT. The non-invasive imaging of MMP activity *in vivo* could have a high impact in basic research as well as in clinical applications. This approach can be established using radiolabeled MMP inhibitors (MMPIs) as tracers for the detection of activated MMPs by means of PET. However, the complexity of diseases associated with dysregulated MMP expression necessitates the imaging of distinct MMPs or MMP subgroups to distinguish their individual role in specific diseases. To this end, selective and potent MMP-13 inhibitors based on a *N*,*N*'-bis(benzyl)pyrimidine-4,6-dicarboxamide core have been synthesized and successfully radiolabeled with carbon-11, fluorine-18 and gallium-68. Selected radiolabeled candidates were evaluated *in vitro* and *in vivo* regarding their pharmacokinetic properties and metabolic stability.

KEYWORDS. Selective matrix metalloproteinase inhibitors, selective MMP-13 inhibitors, positron emission tomography, radiotracer

INTRODUCTION.

Matrix metalloproteinases (MMPs) are a family of structurally and functionally related zinc- and calcium-dependent secreted or membrane anchored endopeptidases. They are involved in many physiological processes like the degradation of extracellular matrix components, tissue remodeling, wound healing, embryotic development, angiogenesis, cell adhesion and proliferation. To date, more than 20 human members of this enzyme class are known, which can be classified based on their substrate specificity into collagenases, gelatinases, stromelysins, membrane-type MMPs, (MT-MMPs) and others. Activated MMPs in the physiological and healthy state are tightly controlled by the endogenous tissue inhibitors of metalloproteinases (TIMPs)[1] Dysregulated MMP expression and activation is i.a. associated with diseases like cancer,[2] atherosclerosis,[3] stroke, arthritis,[4] periodontal disease,[5] multiple sclerosis[6] and cardiovascular disease,[7] in which normal tissue architecture is degraded, disrupted or remodeled. Consequently, the non-invasive imaging of MMP activity *in vivo* could have a high impact in basic research as well as in clinical applications. This approach can be realized by radiolabeled MMP inhibitors (MMPIs) employed as radiotracers for the detection of activated MMPs by means of molecular imaging techniques, such as SPECT (single photon emission computed tomography) and PET (positron emission tomography).

A number of different synthetic MMPIs have been developed and extensively explored in recent years.[8] Despite these promising results the implementation of MMP imaging *in vivo* with radiolabeled MMPIs remains challenging.[9] The complexity of diseases associated with dysregulated MMP expression necessitates the imaging of distinct MMPs or MMP subgroups to distinguish their individual (detrimental or beneficial) role in specific diseases.[10] Classical broad-spectrum MMPIs gain their potency *via* direct interaction with the catalytic zinc(II) ion of the active site of the MMP, with the consequence that MMP selectivity is difficult to

implement into these inhibitors. However, MMPs differ specifically in the S1' pocket in a profound manner, providing an opportunity to gain selectivity.

MMP-13, in particular, possesses a large S1' pocket that, when appropriately occupied by a corresponding ligand, opens up a side pocket (S1'*) not observed in other MMPs. The structural significance of this pocket has been exploited, resulting in potent selective MMP-13 inhibitors, that do not interact with the catalytic zinc.[11,12,13]

MMP-13, the human collagenase-3, is a highly potent secreted protease with broad substrate specificity. The enzyme is not permanently upregulated, but available on demand.[14] Anyway, MMP-13 is the most efficient type II collagen-degrading MMP and responsible for the degradation of cartilage during the development of osteoarthritis and rheumatoid arthritis.[15,16] Osteoarthritis involves the degradation of joints, including articular cartilage and subchondral bone. Like rheumatoid arthritis, which is a chronic inflammatory disease, osteoarthritis is characterized by persistent inflammatory reactions in the joints resulting in a progressive particular destruction associated with the loss of joint function and disability.[17] Therefore, there is a need to explore the aetiology and the pathogenesis of these diseases in an early ("prediseased") state. Early diagnosis and intervention could have a positive clinical as well as a cost effective impact.[18] Although first cloned from human breast carcinoma, MMP-13 has also been found highly up-regulated in other malignant tumors,[19] in chronic wounds,[20] periodontal disease[21] and chronic vascular diseases like arteriosclerosis[22] and aortic aneurysms.[23] The possibility to study disease-related MMP-13 activity *in vivo* by means of PET or SPECT would be of great value to understand the relevance of MMP-13 in such pathologies. To our knowledge, radiolabeled compounds have not been described so far that are selective for MMP-13. The goal of this research is thus the synthesis of a first series of radiolabeled MMP-13 inhibitors and their first *in vitro* and *in vivo* evaluation to estimate their potency for the imaging of MMP-13 activity *in vivo.*

RESULTS AND DISCUSSION

The potent and selective MMP-13 inhibitor *N*,*N*'-bis(4-fluoro-3-methylbenzyl)pyrimidine-4,6-dicarboxamide (**1**) was chosen as lead compound for the design of a number of radiolabeled selective MMP-13 inhibitors (Figure 1, left).[24] This type of inhibitor tolerates modifications of the substituents at the pyrimidine-4,6-dicarboxamide skeletal structure.[25]

The binding modes of the lead structure **1** co-crystallized with MMP-13 are depicted in Figure 1. The ligand fully occupies the S1' pocket and reaches the S1'* pocket with its aromatic residues. This inhibitor does not interact with the catalytic zinc(II) ion in the active center of the enzyme. The central pyrimidine dicarboxamide moiety is the key anchoring point of the molecule and interacts with the amino acids tyrosine 247, 245 and alanine 238. This moiety has to be kept invariant, but modifications of the aromatic residues to enable radiolabeling should be tolerated.

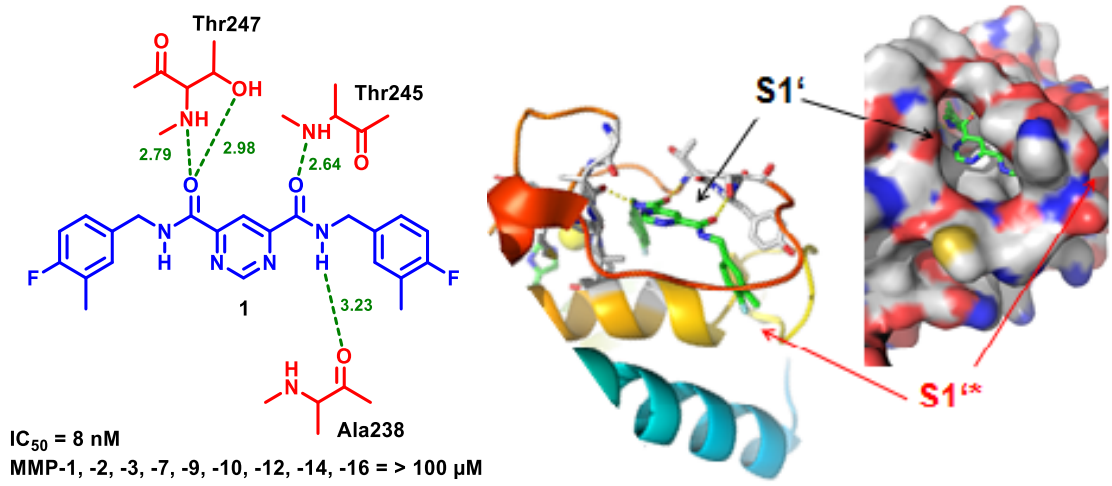

Figure 1. Binding modes of the lead structure *N*,*N*'-bis(4-fluoro-3-methylbenzyl)pyrimidine-4,6-dicarboxamide (**1**) co-crystallized with MMP-13 (PDB ID: 1XUD). Adapted from.[24]

Chemistry. Analogues of **1** were prepared in multi-step organic syntheses and the MMP inhibition potencies for MMP-2, -8, -9, -13 and -14 were examined *in vitro* by fluorometric enzymatic inhibition assays. Modifications of the lead structure are shown in Figure 2. In compound **2** the 4-fluoro-3-methyl benzylamide moiety was maintained at the one side of the molecule, while the other aromatic residue was modified by the introduction of different substituents in *p*-position to enable radiolabeling with carbon-11, fluorine-18 or gallium-68. Literature revealed that an *m*-methoxy substitutent at the benzylamide could improve binding affinities.[25] Analog to compound **2a** and **2b** the second aromatic ring of compound **3** was modified to enable labeling with fluorine-18. Compound **4** represents a combination of both aromatic residues. Radiolabeling can be accomplished *via* direct nucleophilic substitution reaction of the tosylate group by [^{18}F]fluoride (**2b** and **3b**), *via* [^{11}C]methylation of the phenolate **2c**, *via* copper(I) catalyzed click reaction of alkyne **2e** or azide **2f** with [^{18}F]-labeled building blocks or by complexation of the DOTA-chelator with gallium-68 (**2i**).

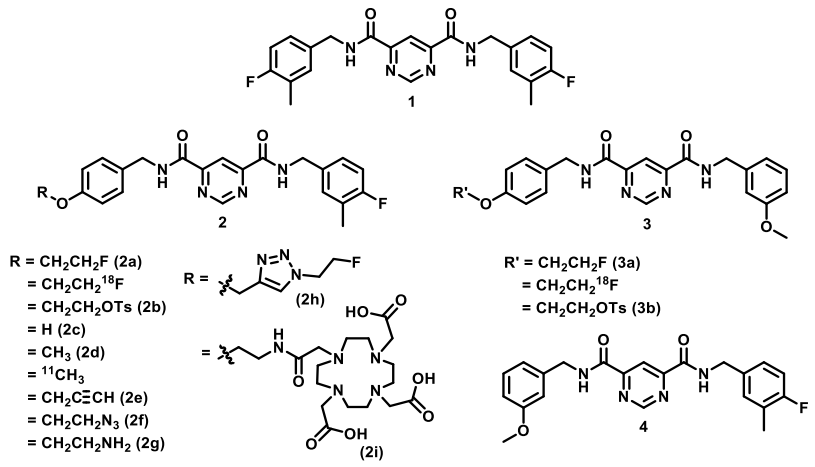

Figure 2. Potent and selective MMP-13 inhibitors including radiolabeling precursors.

The benzylamines used for the synthesis of the MMP-13 inhibitors are represented in Scheme 1. Starting from commercially available 4-hydroxybenzylamine different *p*-substituted benzylamines were prepared by protection of the amine, substitution reaction with 2-fluoroethyl 4-methylbenzenesulfonate,[26] ethane-1,2-diyl bis(4-methylbenzenesulfonate), 2-

azidoethyl 4-methylbenzenesulfonate [27] or 3-bromoprop-1-yne and deprotection of the amine with 4 HCl in dioxane. The alkyne substituted BOC-protected amide **6e** was subjected to a copper(I) catalyzed click reaction with 1-azido-2-fluoroethane.[28] Cleavage of the BOC-protecting group yielded the fluorethyl 1,2,3-triazole-substituted benzylamide **7h**.

Scheme 1. Synthesis of the benzylamines **7a – b**, **e – f** and **7h**.

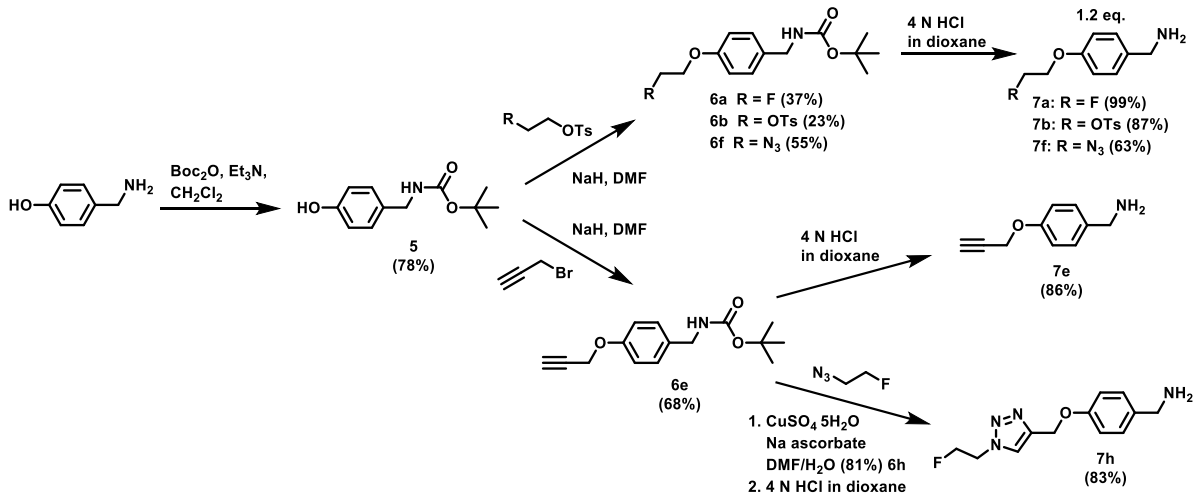

The synthetic strategy of the compound **2** based derivatives **2a**, **b** and **f** bearing a fluoromethylbenzylamide group is depicted in Scheme 2. The organic synthesis started with a potassium permanganate oxidation of 4,6-dimethylpyrimidine and subsequent methylation. Reaction of the resulting dimethyl pyrimidine-4,6-dicarboxylate (**8**) with (4-fluoro-3-methylphenyl)methanamine gave the amide **9**. Deprotection led to the acid **10**, which was converted to the final products *via* coupling reaction with the different benzyl amines (**7a, b** and **f**) using the reagent combination DCC/HOBT (**2a**) or BOP (**2b**, **2f**).

Scheme 2. Synthesis of 4-fluoro-3-methyl benzylamide based MMP-13 inhibitors **2a**, **b** and **f**.

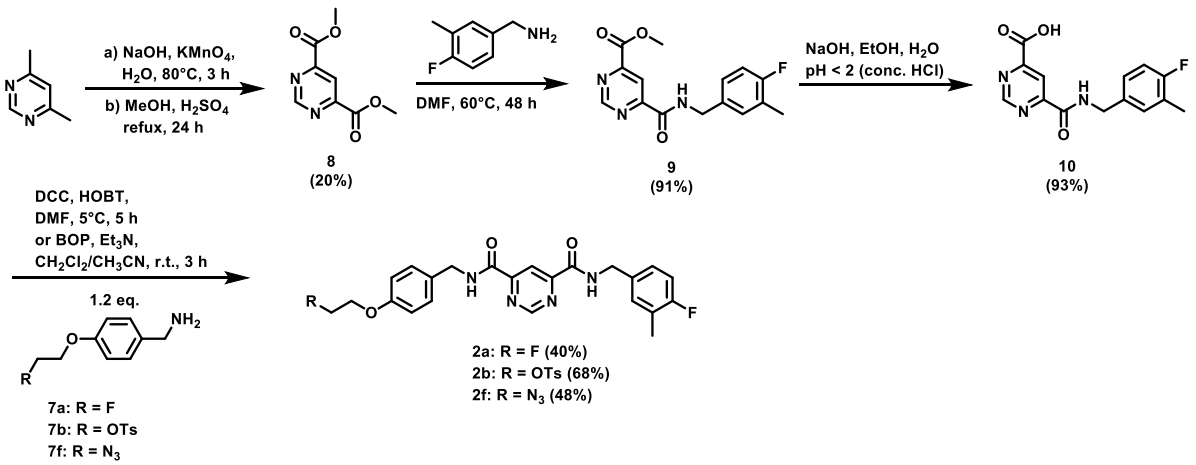

Coupling reaction of acid amide **10** with (3-methoxyphenyl)methanamine gave the pyrimidine dicarboxamide **4**, which represents a combination of both main residues (Scheme 3). Reaction with 4-hydoxybenzylamide led to compound **2c**, the phenolate precursor for carbon-11 labeling with [^{11}C]CH_3I. Methylation of the hydroxyl function with dimethylsulfate and potassium carbonate in acetone provided the non-radioactive reference compound **2d**. To enable radiolabeling *via* copper(I) catalyzed click reaction with fluorine-18 labeled building blocks the alkyne **2e** was synthesized by coupling reaction with BOP. Attempts to receive the triazole compound **2h** applying click chemistry conditions did not lead to the desired product. Copper can be easily chelated by the pyrimidine dicarboxamide moieties in the molecule and therefore it is not available for the click reaction anymore. We observed that even higher amounts of copper(II) sulfate (6 eq.) and sodium ascorbate did not lead to a sufficient conversion. Therefore, the 1,3-dipolar cycloaddiditon was performed starting with the BOC-protected *p*-propylene-substituted benzylamine **6e.** After deprotection the resulting fluoroethyl 1,2,3-triazole-substituted benzylamine was directly subjected to the coupling reaction with acid amide **10**, providing the triazole-substituted product **2h** in a chemical yield of 25%.

Scheme 3. Synthesis of MMP-13 inhibitors **2c-e**, **2h** and **4**.

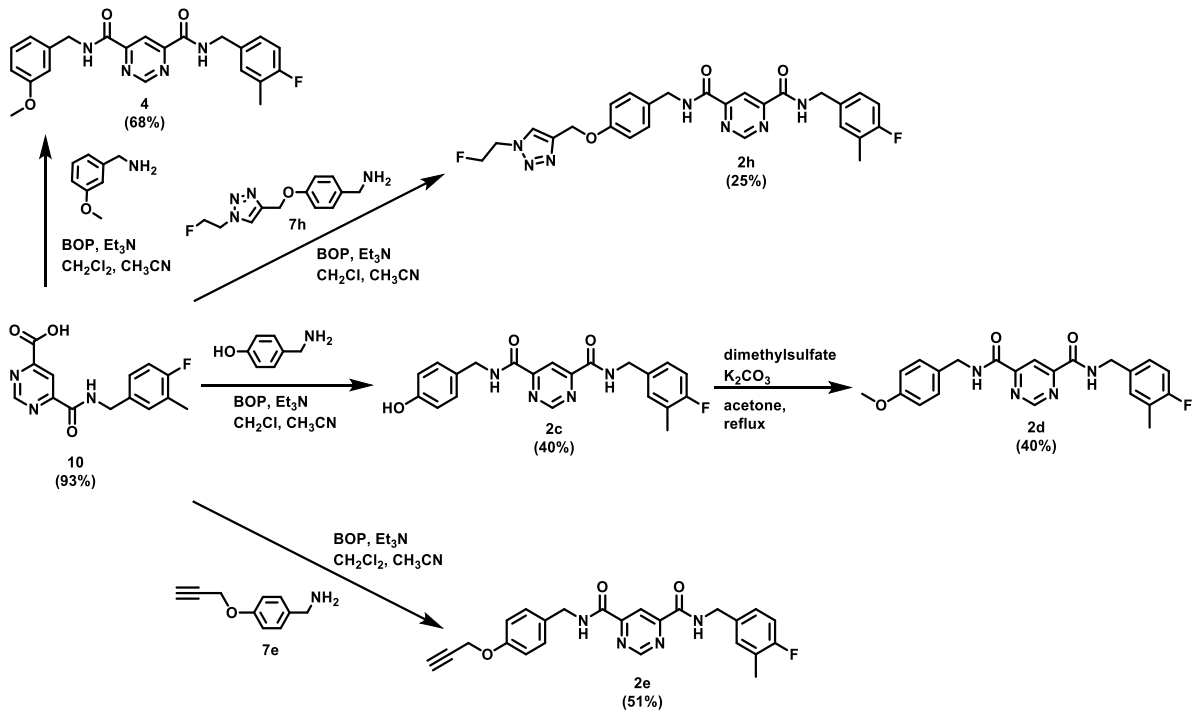

The organic syntheses of compounds **3a** and **3b**, depicted in Scheme 4, were carried out similar to the synthesis of compounds **2a** and **2b** in scheme 2. After oxidation and methylation of 4,6-dimethylpyrimidine, reaction of **8** with (3-methoxyphenyl)methanamine yielded the amide **11**, which was transformed to the carboxylic acid **12** using lithium hydroxide in THF. Conversion of **12** to the corresponding pyrimidine-4,6-dicarboxamides **3a** and **3b** was achieved by coupling with 4-(2-fluoroethoxy)phenylmethane amine (**7a**) or its tosylated analog **7b** using BOP and Et_3N in a dichloromethane/acetonitrile mixture (3:1).

Scheme 4. Synthesis of MMP-13 inhibitors **3a** and **3b**.

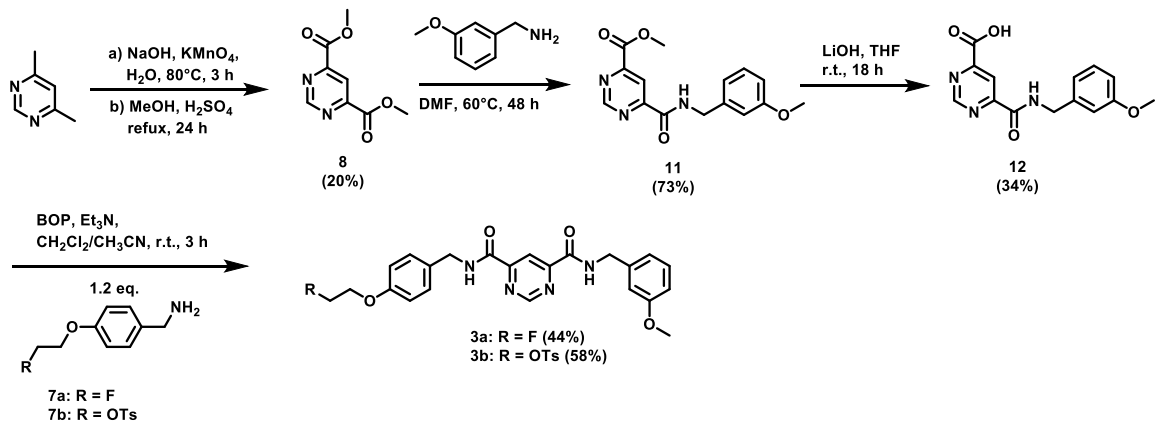

To enable radiolabeling with gallium-68 the DOTA-substituted pyrimidine dicarboxamide derivative **2i** was synthesized (Scheme 5). Reduction of the ethyl azide substituted derivative **2f** with palladium on carbon and H_2 in dry THF provided the amine **2g**. Reaction of the *tert*-butyl protected DOTA-NHS ester in DMF using Et_3N as a base gave the protected DOTA-derivative **13**. Cleavage of the *tert*-butyl groups was achieved with a TFA/water mixture (95:5 v/v) at room temperature in 12 h, yielding the DOTA derivative **2i** in fair yields. Chelating reaction with $Ga(NO_3)_3$ was performed at 55 °C in ammonium acetate buffer (pH 2.2), which was adjusted to pH 3.5 with aqueous HCl.

Scheme 5. Synthesis of the DOTA-derivative **2i** and chelation of gallium.

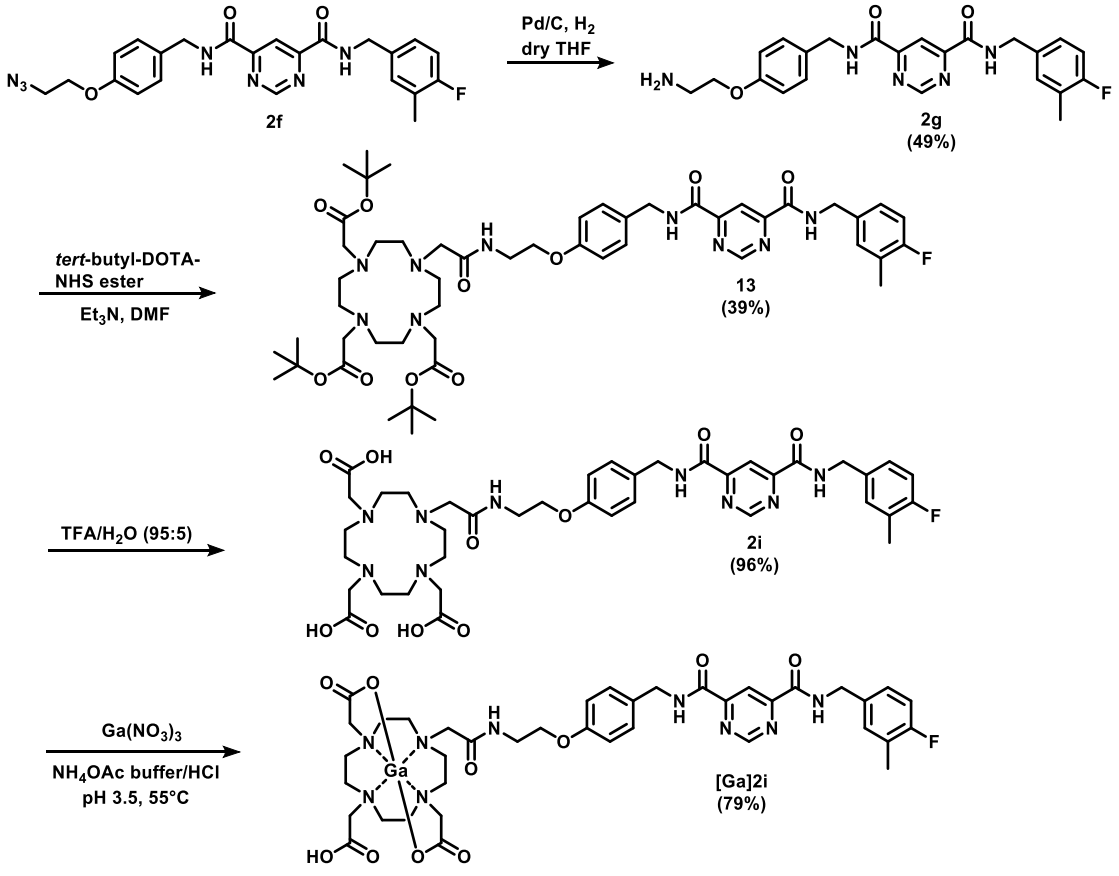

In summary, two series of pyrimidine dicarboxamide based MMP-13 inhibitors with different *p*-substituents at the second aromatic residue were prepared from 4-fluoro-3-methylbenzyl substituted pyrimidine carboxylic acid **10** and from the *m*-methoxybenzyl

substituted pyrimidine carboxylic acid **12**. Fluorinated, methylated and gallium-chelated non-radioactive reference compounds of the potential radioligands **2a**, **2d**, **2h**, **[Ga]2i**, **3a** and **4** were obtained to measure their MMP inhibition potencies by *in vitro* fluorometric assays. ^{18}F-labeling can potentially be accomplished *via* direct nucleophilic substitution reaction of the corresponding tosylate precursors **2b** and **3b** or *via* click reactions with precursors **2f** and **2e** and alkyne or azide based radiosynthons, i.e. 1-azido-2-[^{18}F]fluoroethane and 5-[^{18}F]fluoropent-1-yne. Labeling with carbon-11 can be achieved by [^{11}C]methylation of the hydoxyl precursor **2c**. For labeling with gallium-68 the DOTA derivative **2i** is available.

***In Vitro* Enzyme Assays and clog *D* Values.** The MMP inhibition potencies of the pyrimidine dicarboxamide derivatives **2a**, **2c-i**, **3a** and **4** against activated MMP-2, -8, -9, -13 and -14 were measured by fluorometric *in vitro* inhibition assays following the procedure previously described.[29]

Table 1. MMP inhibition potencies and *c*log *D* (log *D*) values of pyrimidine dicarboxamides **2a, 2c**-**i**, **3a** and **4**.

			IC_{50} [μM][a]		[nM]	log *D* values	
compound	MMP-2	MMP-8	MMP-9	MMP-14	MMP-13	*c*log *D*[b]	log *D* (exp.)[c]
1	>100	>100	41 ± 7	n.d.	226 ± 54 Lit.: 8[24]	4.68	4.83 ± 0.82[24]
2a	>100	>100	>100	n.d.	56 ± 2	4.31	2.77 ± 0.11
2c	>100	>100	>100	>100	8 ± 1	3.44	-
2d	>100	>100	>100	>100	26± 6	4.09	3.34 ± 0.09
2e	>100	>100	>100	>100	0.2 ± 0.05	4.12	-
2f	0.71 ± 0.001	>100	>100	n.d.	14 ± 1	4.06	-
2g	13 ± 1	13 ± 0.1	24 ± 0.2	n.d.	118 ± 0.09	2.85	-
2h	>100	>100	>100	>100	1.8 ± 0.3	3.48	-
2i	17 ± 0.2	14 ± 0.06	23 ± 0.06	n.d.	102 ± 0.1	2.31	-
3a	>100	>100	>100	>100	123 ± 28	3.72	-
4	81 ± 35	>100	>100	>100	159 ± 6	4.09	-

[a] Values are the mean ± SD of three experiments. [b] *c*log *D* values were calculated by ACD/Chemsketch version ACD/Labs 12.00 (log *D* = log *P* at physiological pH (7.4)). [c] log *D* (exp.) value was determined for compounds **[^{18}F]2a**, **[^{18}F]3a** and **[^{11}C]2d** at pH 7.4.

In vitro fluorometric assays of the synthesized compounds revealed good inhibition potencies against MMP-13 and no inhibitory effect against MMP-2, -8, -9 and -14 was observed, with the exception of compounds **2f**, **2g**, **2i**. and **4**. As the lead compound was obtained as a by-product during the syntheses of the (4-fluoro-3-methylbenzyl)amine substituted compounds **2** it was additonally tested in the fluorometric inhibition assays. Two different batches of compound **1** were examined (IC_{50} (MMP-13) = 226 ± 54 nM). Therefore, we assume that all synthesized compounds (**2a**, **2c-e**, **2h**), which reveal equal or higher inhibition potency against MMP-13, are at least as potent as lead stucture **1**.

In summary, modification of one aromatic residue in lead structure **1** is tolerated, when the (4-fluoro-3-methylbenzyl)amide or the (3-methoxybenzyl)amide moiety is maintained in the molecule. All tested compounds showed increased inhibition potencies against MMP-13 compared to lead compound **1** and good (with the exception of compounds **2f**, **2g**, **2i**. and **4**) selectivtiy towards other MMPs tested.

To evaluate the hydrophilic properties of the target compounds, the corresponding calculated log *D* values (*c*log *D*) of the synthesized pyrimidine dicarboxamides are also highlighted in Table 1. Additionally, the partition coefficients (expressed as log *D* values) of the radiolabeled analogs **[^{18}F]2a**, **[^{11}C]2d** and **[^{68}Ga]2i** (see Radiochemistry section) were determined experimentally. The log *D* (exp.) values are lower and differ from the *c*log *D* values (clog *D* (**2a**) = 4.31) in 1.54 units and (*c*log *D* (**2d**) = 4.09) in 0.65 units. Anyhow, the [^{11}C]methylated compound **2d** represents the most lipophilic radiotracer, while the gallium-DOTA derivative (log *D* (exp.) **([^{68}Ga]2i**) = -1.12) shows the highest hydrophilicity.

Radiochemistry. Radiolabeling was performed with the three most clinically prominent PET-radionuclides (^{11}C, ^{68}Ga, ^{18}F) covering the variety of labeling feasibilities on the here presented molecules which we suggest for potential diagnostic PET/CT and PET/MRI.

Synthesis and *in vivo* evaluation of carbon-11 labeled compound [^{11}C]2d. The synthesis of **[^{11}C]2d** was realized by methylation of the phenolic hydroxyl group of precursor **2c** with [^{11}C]CH_3I in the presence of base (Scheme 6). [^{11}C]CO_2 was trapped with $LiAlH_4$ (1 M in THF), forming the lithium methoxide salt, which was then converted to [^{11}C]CH_3I by addition of 60% HI solution in water. The formed [^{11}C]CH_3I was subsequently distilled to the second reaction vial, containing precursor **2c** in DMF in the presence of TBAOH (40% in water). The reaction was performed for 2 min at 80 °C. After semi-preparative HPLC separation and formulation in phosphate buffered saline (7.09 mM) containing 10% of ethanol and 1.6% Polysorbate 80 (Tween® 80). **[^{11}C]2d** was obtained in radiochemical yields in the range of 36 – 50 % and radiochemical purities of > 98% in 29 ± 1 min from the end of radionuclide production. Using starting activities of 6 GBq specific activities in the range of 122 – 330 GBq/μmol were achieved. For the determination of the experimental log *D* value the radioligand was formulated in pure phosphate buffered saline.

Scheme 6. Labeling of **[^{11}C]2d** by [^{11}C]methylation of precursor **2c**.

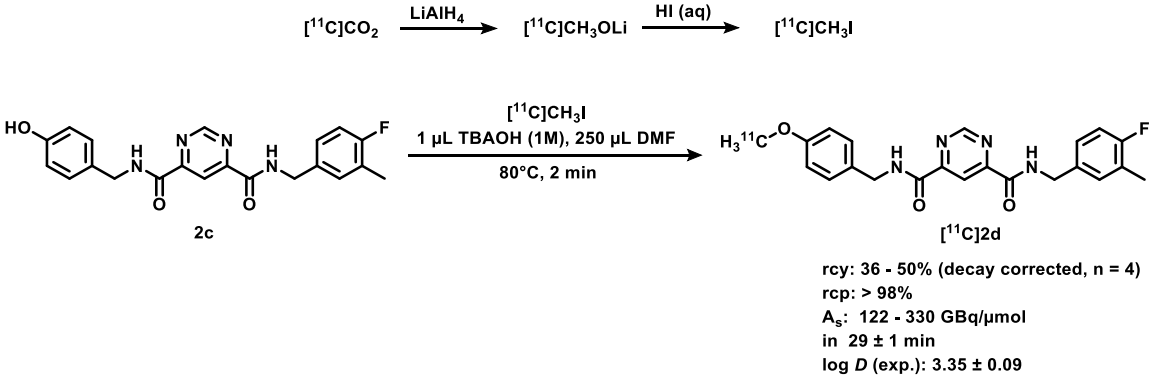

Metabolite analysis. A metabolism study of **[^{11}C]2d** was performed in healthy male balb/c mice using a solid phase extraction method with subsequent HPLC analysis. The animals were intravenously injected (i.v. tail vein) with 50 – 60 MBq of **[^{11}C]2d**. At 15 and 45 min after injection the mice were sacrificed and blood samples were collected immediately from the animals. Analysis of the blood plasma revealed a moderate stability of the radiotracer (Figure 3). The amount of intact **[^{11}C]2d** in plasma was determined to be 89 ± 1% and 38 ± 1% at 15 min and 45 min after injection, respectively (Table 2).

Table 2. Metabolite analysis of **[^{11}C]2d** in plasma.

	Plasma				
	15 min (%)			45 min (%)	
Animal	1	2	3	4	5
Non-polar fraction	92.47	93.37	92.27	61.09	62.88
Intact tracer	88.20	89.92	87.43	37.16	38.87
Non-polar metabolites	4.27	3.45	4.84	23.93	24.01
Polar metabolites	7.53	6.63	7.73	38.91	37.12

n = 3 for 15 min, n = 2 for 45 min

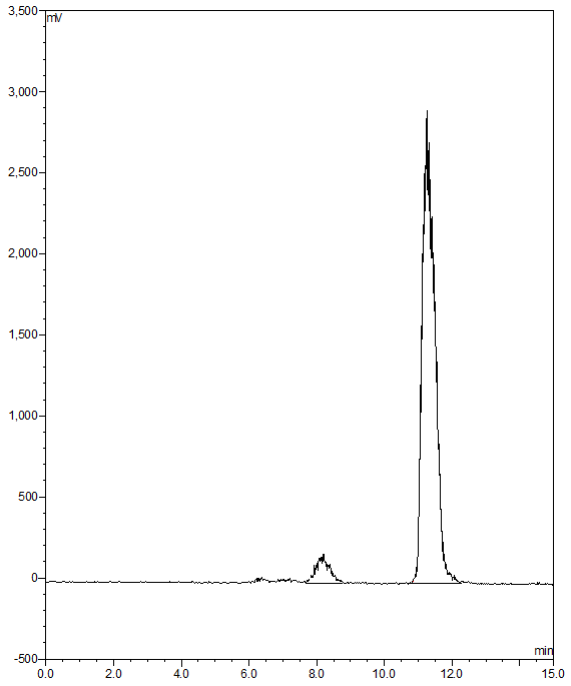

Figure 3. Representative radio-chromatogram of the non-polar fraction after 15 min. t_R**[^{11}C]2d**: 11.25 min.

***Ex vivo* biodistribution.** To evaluate the clearance characteristics of the radioligand **[^{11}C]2d** an *ex vivo* biodistribution study was performed with healthy male balb/c mice (Figure 4). 20 MBq of **[^{11}C]2d** were injected into the tail vein. Mice were sacrificed and dissected at 5, 15, 30 and 60 min p.i.

Overall, **[^{11}C]2d** is cleared quickly and efficiently from the body through hepatic and renal elimination with no significant tracer amounts remaining in non-excreting organs 60 min p.i. High levels of radioactivity were observed in liver and kidneys already 5 min after injection. While the radioactivity in kidneys started to decrease already after 5 min, the liver showed further accumulation of **[^{11}C]2d** until 30 min p.i, due to obviously occurring oxidative phase 1 metabolism, and normal clearance into the intestines. Significant accumulation of the radioactivity in organs/tissues such as brain, heart, lung, muscle and bone, indicating unspecific binding, was not observed. Taken together, **[^{11}C]2d** is predominantly cleared *via* the hepatobiliary excretion route from the liver into the intestines.

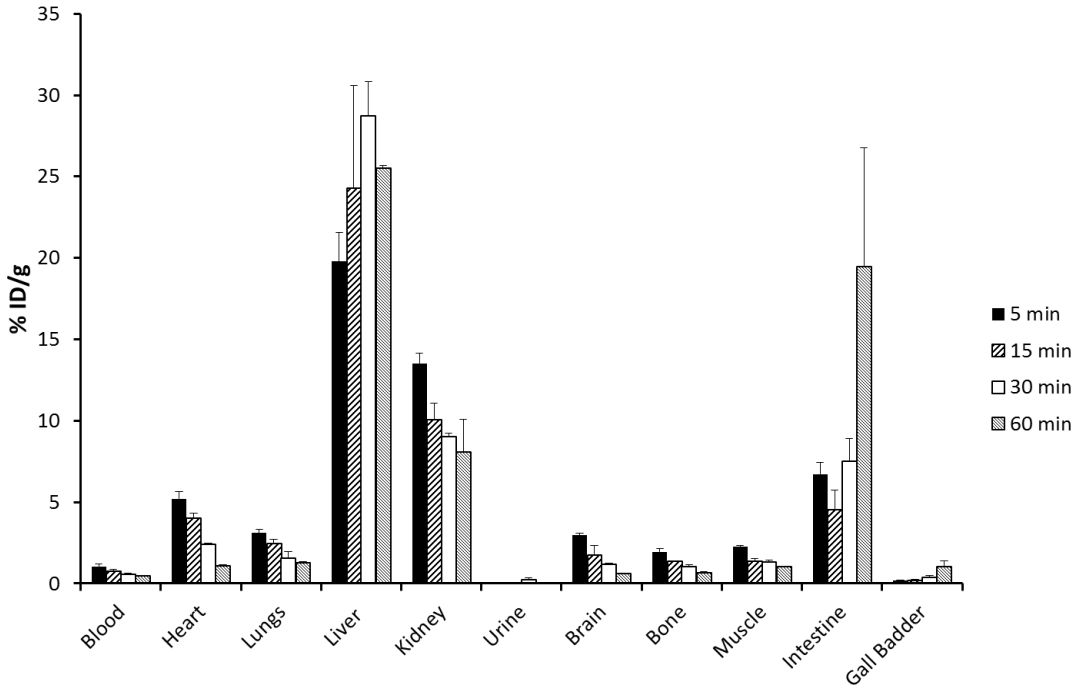

Figure 4. *Ex vivo* biodistribution following intravenous injection of 20 MBq of **[^{11}C]2d** in healthy male balb/c mice (n = 4 for 5 and 30 min, n = 3 for 15 min and 60 min). Data are expressed as percentage injected dose per gram tissue (%ID/g).

***In vivo* biodistribution study.** Additionally, an *in vivo* biodistribution study in adult C57/Bl6 mice after intravenous injection of 400 kBq/g bodyweight of **[^{11}C]2d** was performed as a 60 min dynamic PET scan. Representative coronal whole body images 0 – 10, 30 – 40 and 50 – 60 min after tracer injection are shown in Figure 5.

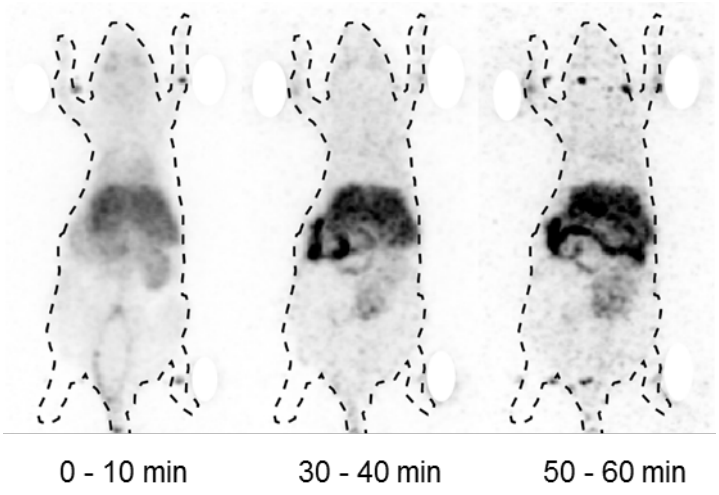

Figure 5: Maximum intensity projections (MIP) of the *in vivo* biodistribution of tracer-associated radioactivity in an adult C57/Bl6 mouse after intravenous injection of **[^{11}C]2d**.

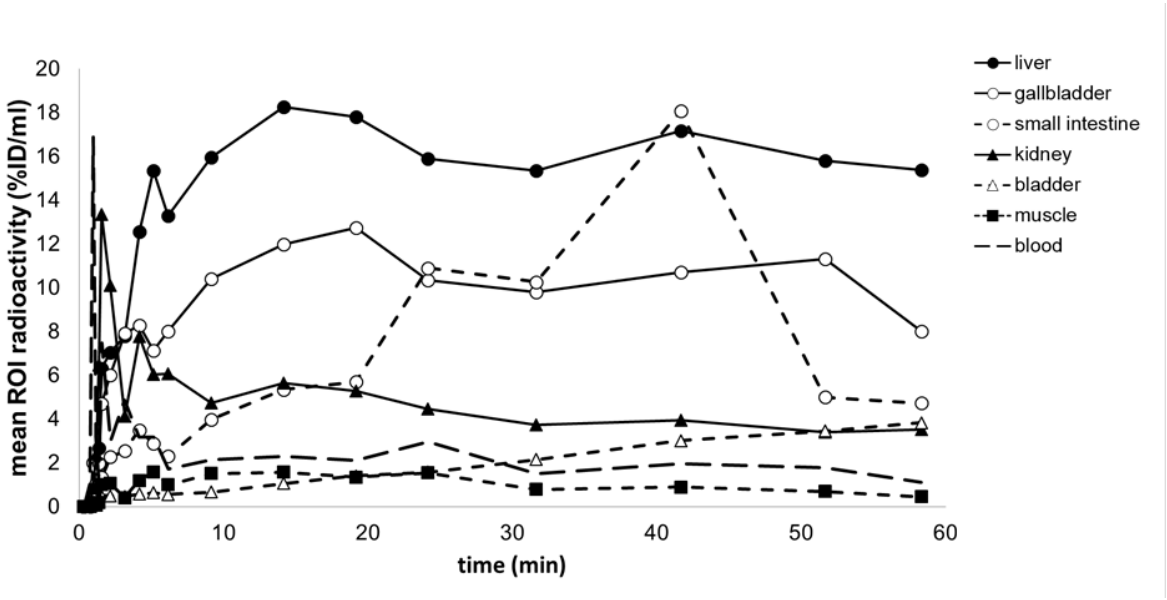

Figure 6. *In vivo* biodistribution of radioactivity in adult C57/Bl6 mouse mice after intravenous injection of **[^{11}C]2d**. Time-activity curves (TACs) illustrate tracer distribution over time in selected regions of interests (ROI). % ID is percentage injected dose.

These data confirm the fast washout of the radioactivity from the blood (T_{max}: 1.6 min, $T_{1/2}$: 0.6 min) and the primarily hepatobiliary excretion route. While the kidneys are cleared very fast (T_{max}: 1.6 min, $T_{1/2}$: 3.3 min), the activity in liver (T_{max}: 14.2 min, $T_{1/2}$: n/a) further accumulates until 14 min and was not significantly eliminated from the liver until the end of the scan (Figure 6).

Synthesis and *in vivo* evaluation of [^{18}F]2a. For imaging of longer time periods radionuclides with adequately longer half-lifes are required. Therefore, the fluorine-18 radiotracer **[^{18}F]2a** was synthesized (Scheme 7). The labeling reaction with fluorine-18 was realized by nucleophilic fluorination of the tosylate precursor **2b** in 15 min at 110 °C using the dried K(K_{222})[^{18}F]F complex in dry DMF. After separation by semi-preparative HPLC, evaporation and formulation the fluorine-18 labeled product was obtained in radiochemical

yields of 21 ± 1% (decay corrected, n = 4) and radiochemical purities of > 98% after 75 ± 2 min from the end of radionuclide production. Determined specific activities were in the range of 18 – 35 GBq/µmol at the end of the radiosynthesis. For *in vivo* biodistribution **[^{18}F]2a** was formulated in 0.9% NaCl/EtOH (9:1 v/v) containing 1.6% of Polysorbate 80. To determine the log *D* values and to study its *in vitro* stability in human blood serum at 37 °C, the radioligand was formulated in phosphate buffered saline.

Scheme 7. Radiolabeling of **[^{18}F]2a** *via* direct nucleophilic substitution reaction with [^{18}F]fluoride.

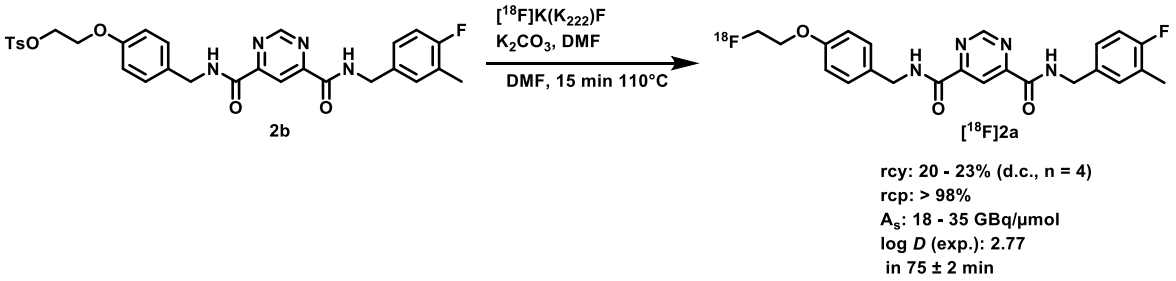

***In Vivo* Biodistribution Study.** Representative coronal whole body images 0 – 10, 30 – 40, 50 – 60 and 80 – 90 min after injection of **[^{18}F]2a** in adult C57/BL6 mice are shown in Figure 7.

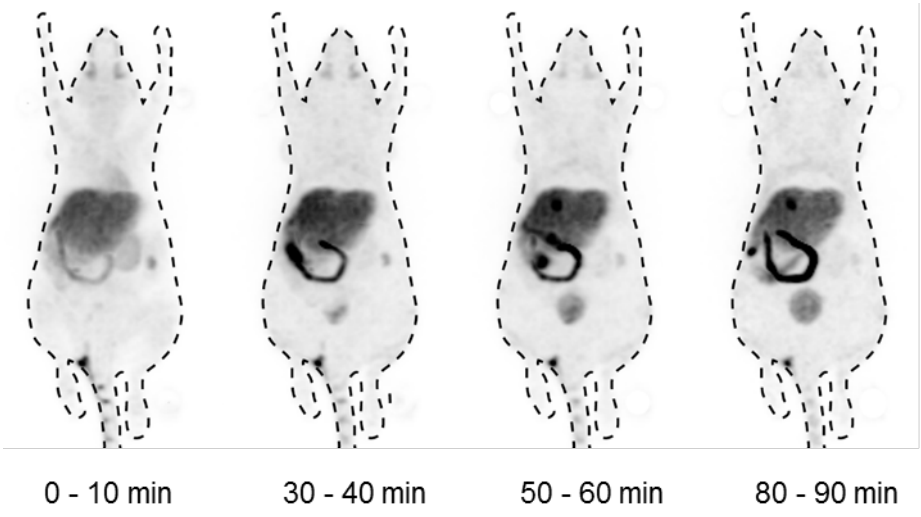

Figure 7. Maximum intensity projection (MIPs) of the *in vivo* biodistribution of tracer-associated radioactivity in an adult C57/Bl6 mouse after intravenous injection of **[^{18}F]2a**.

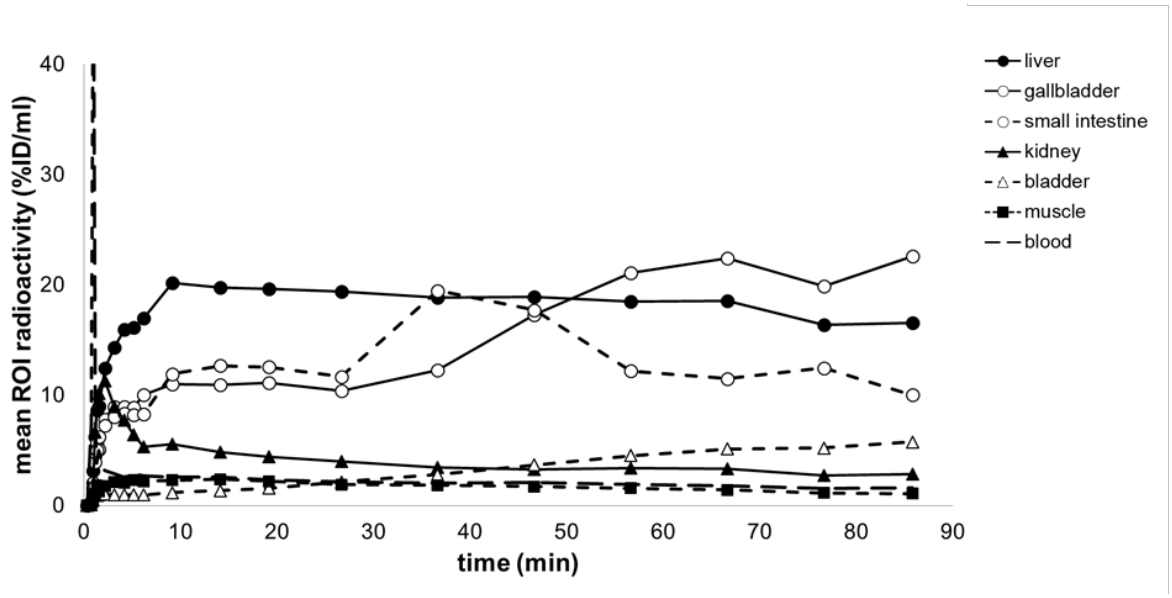

Figure 8. *In vivo* biodistribution of radioactivity in adult C57/Bl6 mouse after intravenous injection of **[^{18}F]2a**. Time-activity curves (TACs) illustrate tracer distribution over time in selected regions of interests (ROI). %ID: percentage injected dose.

Overall, the fluorine-18 labeled radioligand **[^{18}F]2a** showed a similar biodistribution behavior as compared to the carbon-11 labeled tracer **[^{11}C]2d**. Clearance from blood is fast (T_{max}: 1.0 min, $T_{1/2}$: 0.2 min) and no significant remaining tracer amounts were observed in non-excreting organs 90 min. p.i.. The kidneys are also cleared very fast (T_{max}: 2.2 min, $T_{1/2}$: 7 min), while the activity in the liver further accumulated (T_{max}: 9.2 min, $T_{1/2}$: n/a). Similar to **[^{11}C]2d** the activity in the liver was not eliminated until the end of the scan. Defluorination of the radioligand *in vivo*, expected to be indicated by bone uptake, was not observed in the entire imaging study. Furthermore accumulation of **[^{18}F]2a** in organs/tissues such as brain, heart, lung and muscle, normally indicating unspecific binding, was not detected (Figure 8).

Altogether, both radiotracers **[^{11}C]2d** and **[^{18}F]2a** showed a predominant hepatobiliary excretion with remaining tracer accumulation over time in the liver. Aiming to increase the

water solubility of the tracer thereby improving the clearance characteristics the more hydrophilic DOTA conjugate **2i** was constructed and labeled with gallium-68 and evaluated *in vivo*.

Synthesis and *in vivo* evaluation of [^{68}Ga]2i. Radiolabeling of the DOTA conjugate **2i** was performed on an iQS® Ga-68 Fluidic Labeling Module (itg) with an integrated itg Ge-68/Ga-68 generator. The labeling reaction was carried out in NH_4OAc/HCl buffer (pH 3.5 – 4) for 10 min at 105 °C. After HPLC separation, evaporation and formulation in phosphate buffered saline the product was obtained in radiochemical yields of 73 ± 5% (decay corrected, n = 4) with radiochemical purities > 99% and specific activities of 18 ± 2% in 74 ± 1 min. The identity of the product was confirmed with analytical HPLC by coinjection of **[^{68}Ga]2i** and the non-labeled compound **[Ga]2i**. The log *D* value was experimentally determined to be -1.12 ± 0.06.

An *in vivo* biodistribution study in adult C57/Bl6 mice after intravenous injection of 400 kBq/g bodyweight of **[^{11}Ga]2i** was performed as 90 min dynamic PET scan. Representative coronal whole body images 0 – 10 min, 30 – 40 min, 50 – 60 min and 80 – 90 min after tracer injection are shown in Figure 9.

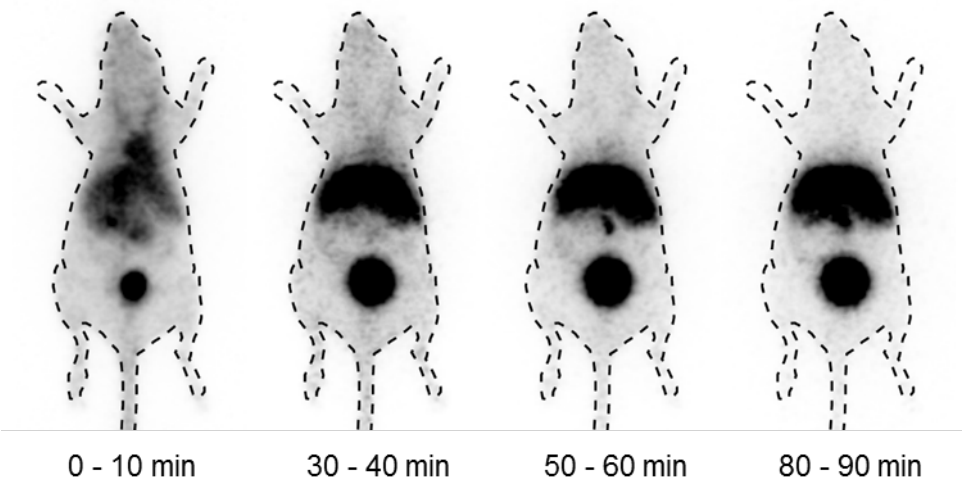

Figure 9. Maximum intensity projections (MIPs) of the *in vivo* biodistribution of tracer-associated radioactivity in an adult C57/Bl6 mouse after intravenous injection of **[^{68}Ga]2i**.

Overall, **[^{68}Ga]2i** is cleared from the body through hepatobiliary and renal elimination with no tracer amounts remaining in non-excreting organs 90 min p.i. Accumulation of **[^{68}Ga]2i** in organs/tissues such as brain, lung and muscle was not observed (Figure 10).

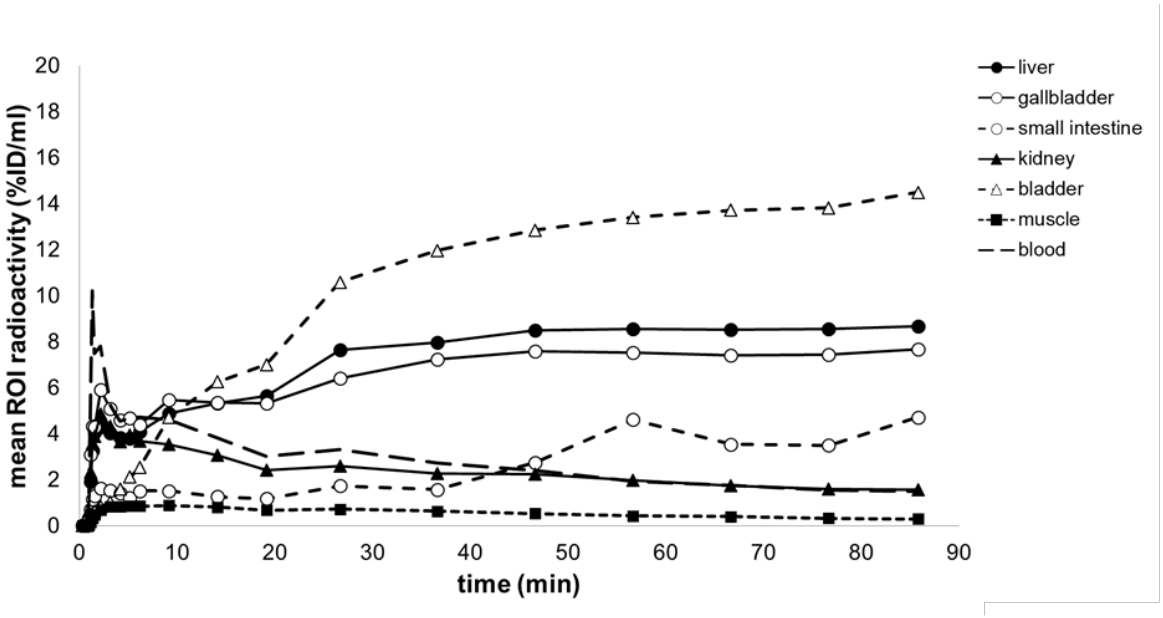

Figure 10. *In vivo* biodistribution of radioactivity in an adult C57/Bl6 mouse after intravenous injection of **[^{68}Ga]2i**. Time-activity curves (TACs) illustrate tracer dynamics in selected regions of interest (ROI). %ID: percentage injected dose.

In comparison to the carbon-11 and the fluorine-18 radioligands the more hydrophilic gallium-68 tracer **[^{68}Ga]2i** shows an enhanced blood retention time. First clearance from the blood occurs fast (T_{max}: 1.4 min, $T_{1/2}$: 2.6 min), but then the activity from whole body was washed out slowly. Up to 30-40 min p.i. radioactivity is present in the blood stream and the two jugular veins are still visible in the PET scan at these time points. Additionally a shift towards a renal clearance was observed. The ratio of the activity in bladder and liver is nearly 1:1. But after an observation time of 90 min there was still no elimination from the liver

visible (T_{max}: 56.7 min, $T_{1/2}$: n/a during observation). Therefore we assume that the tracer somehow accumulates in the liver, obviously due to phase 1 and 2 metabolism.

CONCLUSION

Based on the lead structure *N*,*N*'-bis(4-fluoro-3-methylbenzyl)pyrimidine-4,6-dicarboxamide selective and potent MMP-13 inhibitors have been successfully synthesized and radiolabeled with carbon-11, fluorine-18 and gallium-68. First *in vivo* evaluation of **[^{11}C]2d** showed moderate metabolic stability in plasma and a primarily hepatobiliary excretion route in biodistribution studies. Clearance from the liver occurred relatively slow. A similar behavior was found for the fluorine-18 labeled radioligand **[^{18}F]2a**. No defluorination or unspecific binding was observed for this MMP-13 targeted radioligand. The more hydrophilic [^{68}Ga]-DOTA derivative **[^{68}Ga]2i** revealed a longer blood retention time. A shift towards renal clearance was determined with a balanced excretion through the hepatobiliary and renal routes. Nearly no elimination of the **[^{68}Ga]2i** tracer-associated activity from the liver was detected 90 min p.i..

The here described radiolabeled selective MMP-13 inhibitors are potential PET tracers for the *in vivo* imaging of MMP-13. Due to the fact, that MMP-13 is overexpressed under pathological condition, these radiotracers could enable earlier and more specific diagnosis of several MMP-13 related diseases. Therefore, preclinical evaluation of these radiotracers by means of small animal PET/CT and corresponding murine disease models characterized by up regulated levels of MMP-13, e.g. models of breast cancer and arthritis are planned.

EXPERIMENTAL SECTION

General. All chemicals, reagents and solvents for the synthesis of the compounds were analytical grade, purchased from commercial sources and used without further purification unless otherwise specified. All air and moisture-sensitive reactions were performed under

argon atmosphere. Solvents were purified and dried by literature methods where necessary. The melting points (mp) are uncorrected and were determined in capillary tubes on a Stuart Scientific SMP3 capillary melting point apparatus. Column chromatography was performed on Merck silica gel 60 (0.040 – 0.063 mm). Thin layer chromatography (TLC) was carried out on silica gel-coated polyester TLC plates (Polygram, SIL G/UV_{254}, Macherey-Nagel) using solvent mixtures of cyclohexane (CH), ethyl acetate (EA) and methanol (MeOH). Compounds were visualized by UV light (254 nm). NMR spectra were recorded in $CDCl_3$, CD_3OH or DMSO-d_6 on a Bruker ARX300, a Bruker DPX300 (^{1}H NMR, 300 MHz, ^{13}C NMR, 75MHz, ^{19}F NMR, 282 MHz), a Bruker AMX 400 (^{1}H NMR, 400 MHz, ^{13}C NMR, 100 MHz) and a Varian Unity plus 600 (^{1}H NMR, 600 MHz, ^{13}C NMR, 151 MHz) spectrometer. TMS (^{1}H), $CDCl_3$, DMSO-d_6, CD_3OD (^{13}C) and $CFCl_3$ (^{19}F) were used as internal standards and all chemical shift values were recorded in ppm (δ). Exact mass analyses were conducted on a Bruker MicroTof apparatus. The chemical purities of each new non-radioactive compound were ≥ 95% and assessed by analytical gradient reversed-phase HPLC system **A** or **B** (λ=254 nm). HPLC System **A**: Two Smartline 1000 pumps and a Smartline UV detector 2500 (Herbert Knauer GmbH), a GabiStar γ-detector (Raytest Isotopenmessgeräte GmbH, Elysia) and a Nucleosil 100-5 C-18 column (250 mm × 4.6 mm). The recorded data were processed by the GINA Star software (Raytest Isotopenmessgeräte GmbH, Elysia). The HPLC method **A1** started with a linear gradient from 10% to 90% CH_3CN in water (0.1% TFA) over 9 min, followed by a linear gradient from 90% to 10% CH_3CN in water (0.1% TFA) over 6 min, with a flow rate of 1 mL·min^{-1} (unless otherwise specified). HPLC method **A2** started with 35% CH_3CN in water (0.1% TFA) for 13 min, followed by a linear gradient from 35% to 90% CH_3CN in water (0.1% TFA) over 2 min, followed by a linear gradient from 90% to 35% CH_3CN in water (0.1% TFA) over 3 min with a flow rate of 1 mL·min^{-1}. HPLC method **A3** started isocratically with 60% CH_3CN in water (0.1% TFA) for 9 min, followed by a linear gradient from 60% to 90% CH_3CN in water (0.1% TFA) over 3 min, followed by a linear

gradient from 90% to 60% CH_3CN in water (0.1% TFA) over 3 min with a flow rate of 1 $mL \cdot min^{-1}$. HPLC system **B**: Two K-1800 pumps and an S-2500 UV detector (Herbert Knauer GmbH), a GabiStar γ-detector (Raytest Isotopenmessgeräte GmbH, Elysia). The recorded data were processed by the ChromGate HPLC software (Herbert Knauer GmbH). HPLC method **B1** using a Nucleosil 100-5 C18 column (250 mm × 4.6 mm) started with a linear gradient from 10% to 80% CH_3CN in water (0.1% TFA) over 18 min, holding for 20 min and followed by a linear gradient from 80% to 10% CH_3CN in water (0.1% TFA) over 2 min, with a flow rate of 1.5 $mL \cdot min^{-1}$. HPLC method **B2** using a Eurospher column (100 C18, 250 mm × 20 mm) started with a linear gradient from 10% to 80% CH_3CN in water (0.1% TFA) over 18 min, holding for 20 min and followed by a linear gradient from 90% to 10% CH_3CN in water (0.1% TFA) over 2 min, with a flow rate of 7.0 $mL \cdot min^{-1}$. Dimethyl pyrimidine-4,6-dicarboxylate[30] 2-azidoethyl 4-methylbenzenesulfonate,[31]**Fehler! Textmarke nicht definiert.** 1-azido-2-fluoroethane,[32] and 2-fluoroethyl 4-methylbenzenesulfonate[33] were synthesized following literature procedures. All animal experiments were approved by the North Rhine-Westphalia Agency for Nature, Environment, and Consumer Protection (Landesamt für Natur, Umwelt und Verbraucherschutz Nordrhein-Westfalen-LANUV).

Dimethyl pyrimidine-4,6-dicarboxylate (8). A white solid, yield: 20%, mp 80 °C, analytical data see ref. [30].

Methyl 6-((4-fluoro-3-methylbenzyl)carbamoyl)pyrimidine-4-carboxylate (9). To a solution of dimethyl pyrimidine-4,6-dicarboxylate (**8**, 1.31 g, 6.86 mmol) in DMF (25 mL) (4-fluoro-3-methylphenyl)methanamine (0.95 g, 6.86 mmol) was added. After being stirred for 48 h at 60 °C, the solvent was removed under reduced pressure. The residue was redissolved in EA (200 mL) and washed with saturated aqueous $NaHCO_3$ (50 mL), 0.5 N aqueous HCl (50 mL) and water (50 mL). After being dried over magnesium sulfate, the solvent was removed under reduced pressure. The product was purified by column chromatography (silica

gel, CH/EA 2:1) and obtained as a grey oil (1.96 g, 6.45 mmol, 91%). ^{1}H NMR (300 MHz, CD_3OD) δ 9.38 (s, pyrimidineAr*H*, 1H), 8.81 (d, pyrimidineAr*H*, 1H), 8.25 (t, N*H*, $^{3}J_{H,H}$ = 5.7 Hz, 1H), 7.22 – 7.10 (m, Ar*H*, 2H), 6.98 (m, Ar*H*, 1H), 4.62 (d, NHCH_2, $^{3}J_{H,H}$ = 6.0 Hz, 2H), 4.08 (s, CO_2CH_3, 3H), 2.27 (d, ArCH_3, $^{4}J_{H,F}$ = 1.8 Hz, 3H). ^{13}C NMR (75 MHz, CD_3OD) δ 163.77 (*C*ONH), 161.65 (*C*OOMe), 160 87 (d, Ar*C*F, $^{1}J_{C,F}$ = 245.1 Hz), 158.67 (pyrimidineAr*C*H), 158.09 (pyrimidineAr*C*CONH), 157.00 (pyrimidineAr*C*COMe), 132.72 (d, Ar*C*CH_2, $^{3}J_{C,F}$ = 3.6 Hz), 131.11 (d, Ar*C*H, $^{4}J_{C,F}$ = 5.4 Hz), 126.83 (d, Ar*C*H, $^{3}J_{C,F}$ = 8.2 Hz), 125.36 (d, Ar*C*CH_3, $^{2}J_{C,F}$ = 17.6 Hz), 118.45 (pyrimidineAr*C*H), 115.28 (d, Ar*C*H, $^{2}J_{C,F}$ = 22.6 Hz), 53.63 (CO_2CH_3), 43.09 (NH*C*H_2), 14.53 (d, Ar*C*H_3, $^{3}J_{C,F}$ = 3.5 Hz). HRMS-ES-EM: *m/z* = 326.0906 [$(M+Na)^+$] calcd for $C_{15}H_{14}FN_3O_3Na^+$: 326.0911.

6-((4-Fluoro-3-methylbenzyl)carbamoyl)pyrimidine-4-carboxylic acid (10). To a solution of methyl 6-((4-fluoro-3-methylbenzyl)carbamoyl)pyrimidine-4-carboxylate (**9**, 1.80 g, 5.93 mmol) in ethanol (45 mL) sodium hydroxide (0.26 g, 6.52 mmol), dissolved in water (1.8 mL), was added. The reaction was stirred at room temperature for 3 h. After complete conversion, as indicated by TLC, the solvent was removed under reduced pressure. Water (100 mL) was added and the pH was adjusted to pH < 2 with concentrated aqueous HCl. The suspension was filtered and the precipitate dried *in vacuo*. Column chromatographic purification (silica gel, CH/EA 2:1) yielded the product as colorless oil (1.59 g, 5.51 mmol, 93%). ^{1}H NMR (300 MHz, CD_3OD) δ 9.37 (d, pyrimidineAr*H*, $^{5}J_{H,H}$ = 1.4 Hz, 1H), 8.70 (d, pyrimidineAr*H*, $^{5}J_{H,H}$ = 1.3 Hz, 1H), 7.18 (m, Ar*H*, 1H), 7.13 (m, Ar*H*, 1H), 6.90 (m, Ar*H*, 1H), 6.93 (m, Ar*H*, 1H), 4.56 (s, NHCH_2Ar, 2H), 2.22 (s, ArCH_3, 3H). ^{13}C NMR (75 MHz, $CDCl_3$) δ 164.91 (*C*OOH), 163.78 (*C*ONH), 161 72 (d, Ar*C*F, $^{1}J_{C,F}$ = 243.2 Hz), 160.33 (pyrimidineAr*C*COH), 159.24 (pyrimidineAr*C*H), 157.81 (pyrimidineAr*C*CONH), 132.67 (d, Ar*C*CH_2, $^{3}J_{C,F}$ = 3.7 Hz), 131.81 (d, Ar*C*H, $^{4}J_{C,F}$ = 5.1 Hz), 127.69 (d, Ar*C*H, $^{3}J_{C,F}$ = 8.2 Hz), 125.75 (d, Ar*C*CH_3, $^{2}J_{C,F}$ = 17.5 Hz), 119.07 (pyrimidineAr*C*H), 115.71 (d, Ar*C*H, $^{2}J_{C,F}$ =

22.6 Hz), 43.54 (NH*C*H$_2$), 14.54 (d, Ar*C*H$_3$, $^3J_{C,F}$ = 3.6 Hz). HRMS-ES-EM: *m/z* = 288.0790 [(M-H)$^-$] calcd for $C_{14}H_{11}FN_3O_3^-$: 288.0790. HRMS-ES-EM: *m/z* = 290.0935 [(M+H)$^+$] calcd for $C_{14}H_{11}FN_3O_3^+$: 290.0935.

***N*^{4}-(4-Fluoro-3-methylbenzyl)-*N*^{6}-(4-(2-fluoroethoxy)benzyl)pyrimidine-4,6-dicarboxamide (2a).** 6-((4-Fluoro-3-methylbenzyl)carbamoyl)pyrimidine-4-carboxylic acid (**10**, 32.4 mg, 0.11 mmol, 1.2 eq.) and (4-(2-fluoroethoxy)phenyl)methanamine (**7a**, 14.5 mg, 0.09 mmol, 1.0 eq.) were dissolved in DMF (2 mL) and the reaction mixture was cooled to 5 °C. Subsequently, *N*,*N*'-dicyclohexylcarbodiimide (DCC, 21.2 mg, 0.10 mmol, 1.1 eq.) and hydroxybenzotriazole (HOBt, 12.6 mg, 0.09 mmol, 1.0 eq.) were added and the mixture was stirred for 5 h at 5 °C. After being stirred for another 12 h at room temperature, the precipitate was filtered off and the solvent was removed under reduced pressure. The residue was redissolved in EA, washed with saturated aqueous $NaHCO_3$ (50 mL) and water (50 mL) and dried over magnesium sulfate. The solvent was removed under reduced pressure and the product was purified by HPLC using HPLC system **B**, method **B2**. The product was obtained as a colorles solid (15.9 mg, 0.04 mmol, 40%); mp 113 °C. ^{1}H NMR (300 MHz, $CDCl_3$) δ 9.16 (s, pyrimidineAr*H*, 1H), 8.94 (s, pyrimidineAr*H*, 1H), 8.20 (d, N*H*, $^3J_{H,H}$ = 6.1 Hz, 2H), 7.30 (d, Ar*H*, $^3J_{H,H}$ = 8.6 Hz, 2H), 7.22 – 7.09 (m, Ar*H*, 2H), 7.03 – 6.94 (m, ArH, 1H), 6.92 (d, $^3J_{H,H}$ = 8.6 Hz, 2H), 4.76 (dm, CH$_2$C*H*$_2$F, $^2J_{H,F}$ = 47.4 Hz, 2H), 4.63 (d, NHC*H*$_2$, $^3J_{H,H}$ = 5.7 Hz, 2H), 4.61 (d, NHC*H*$_2$, $^3J_{H,H}$ = 5.8 Hz, 2H), 4.21 (dm, C*H*$_2$CH$_2$F, $^3J_{H,F}$ = 27.9 Hz, 2H), 2.26 (s, ArC*H*$_3$, 3H). ^{13}C NMR (75 MHz, $CDCl_3$) δ 161.81 (*C*ONH), 161.73 (*C*ONH), 160 76 (d, Ar*C*F, $^1J_{C,F}$ = 259.0 Hz), 158.83 (pyrimidineAr*C*H), 158.69 (pyrimidineAr*C*H), 158.06 (pyrimidineAr*C*CONH), 156.58 (Ar*C*CO), 132.87 (d, Ar*C*CH$_2$, $^3J_{C,F}$ = 3.8 Hz), 131.14 (d, Ar*C*H, $^4J_{C,F}$ = 5.3 Hz), 130.15 (Ar*C*O), 129.39 (Ar*C*H), 126.85 (d, Ar*C*H, $^3J_{C,F}$ = 8.2 Hz), 116.28 (Ar*C*CH$_2$), 115.25 (d, Ar*C*H, $^2J_{C,F}$ = 22.6 Hz), 114.92 (pyrimidineAr*C*H), 81.87 (d, *C*H$_2$CH$_2$F, $^1J_{C,F}$ = 170.8 Hz), 67.16 (d, *C*H$_2$CH$_2$F, $^3J_{C,F}$ = 20.5 Hz), 43.17 (NH*C*H$_2$), 43.05

(NH*C*H$_2$), 14.53 (d, Ar*C*H$_3$, $^2J_{C,F}$ = 3.7 Hz). ^{19}F NMR (282 MHz, CDCl$_3$) δ -118.86 (m, 1F), 223.84 (tt, $^2J_{H,F}$ = 47.4 Hz, $^3J_{H,F}$ = 27.8 Hz, 1F). HRMS-ES-EM: *m/z* = 463.1557 [(M+Na)$^+$] calcd for $C_{23}H_{22}F_2N_4O_3Na^+$: 463.1552. HPLC system **B**, method **B1**: t_R =18.90 min (> 99%).

2-(4-((6-((4-Fluoro-3-methylbenzyl)carbamoyl)pyrimidine-4-carboxamido)methyl)-phenoxy)ethyl 4-methylbenzenesulfonate (2b). 6-((4-Fluoro-3-methylbenzyl)carbamoyl)pyrimidine-4-carboxylic acid (**10**, 15.0 mg, 0.052 mmol, 1.0 eq.) and 2-(4-(aminomethyl)phenoxy)ethyl 4-methylbenzenesulfonate (**7b**, 20.0 mg, 0.062 mmol, 1.2 eq.) were dissolved in a dichloromethane/acetonitrile mixture (0.8 mL, 3:1). Dry triethylamine (22 µL, 0.156 mmol, 3 eq.) and (benzotriazole-1-yloxy)tris(dimethylamino)phosphonium hexafluorophosphate (23 mg, 0.052 mmol, 1.0 eq.) were added and the reaction mixture was stirred for 12 h at room temperature. The solvent was removed under reduced pressure and the residue was purified by column chromatography (silica gel, CH/EA 1:1). The product was obtained as a colorless solid (21.0 mg, 0.035 mmol, 68%); mp 40 °C. ^{1}H NMR (250 MHz, CDCl$_3$) δ 9.16 (d, pyrimidineAr*H*, $^5J_{H,H}$ = 1.0 Hz 1H), 8.92 (d, pyrimidineAr*H*, $^5J_{H,H}$ = 1.0 Hz 1H), 8.31 – 8.07 (m, N*H*, 2H), 7.81 (d, Ar*H*, $^3J_{H,H}$ = 8.3 Hz, 2H), 7.34 (d, Ar*H*, $^3J_{H,H}$ = 8.1 Hz, 2H), 7.24 (d, Ar*H*, $^3J_{H,H}$ = 8.5 Hz, 2H), 7.21 – 7.07 (m, Ar*H*, 2H), 6.97 (m, Ar*H*, 1H), 6.77 (d, $^3J_{H,H}$ = 8.6 Hz, 2H), 4.61 (s, NHC*H*$_2$, 2H), 4.59 (s, NHC*H*$_2$, 2H), 4.35 (dd, CH$_2$C*H*$_2$O, $^3J_{H,H}$ = 5.6 Hz, $^3J_{H,H}$ = 3.8 Hz, 2H), 4.13 (dd, C*H*$_2$CH$_2$O, $^3J_{H,H}$ = 5.6 Hz, $^3J_{H,H}$ = 3.8 Hz, 2H), 2.44 (s, ArC*H*$_3$, 3H), 2.26 (d, ArC*H*$_3$, $^4J_{H,F}$ = 1.7 Hz, 3H). ^{13}C NMR (63 MHz, CDCl$_3$) δ 161.81 (*C*ONH), 161.74 (*C*ONH), 160 83 (d, Ar*C*F, $^1J_{C,F}$ = 244.8 Hz), 158.78 (pyrimidineAr*C*), 158.69 (pyrimidineAr*C*), 156.58 (pyrimidineAr*C*H), 157.62 (Ar*C*OCH$_2$), 144.97 (Ar*C*CH$_3$), 132.86 (d, Ar*C*CH$_2$, $^4J_{C,F}$ = 3.6 Hz), 132.83 (Ar*C*CH$_2$), 131.12 (d, Ar*C*H, $^3J_{C,F}$ = 5.3 Hz), 130.29 (Ar*C*SO$_2$), 129.84 (Ar*C*H), 129.31 (Ar*C*H), 127.98 (Ar*C*H), 126.83 (d, Ar*C*H, $^3J_{C,F}$ = 8.2 Hz), 125.30 (ArCH, $^2J_{C,F}$ = 17.5 Hz), 116.25 (pyrimidineAr*C*H), 115.24 (d, Ar*C*H, $^2J_{C,F}$ = 22.6 Hz), 114.83 (Ar*C*H), 68.02

(CH_2CH_2O), 65.49 (CH_2CH_2O), 43.11 ($NHCH_2$), 43.04 ($NHCH_2$), 14.51 (d, $ArCH_3$, $^2J_{C,F}$ = 3.5 Hz). ^{19}F NMR (282 MHz, $CDCl_3$) δ -117.05 (m, 1F). HRMS-ES-EM: *m/z* = 593.1870 [$(M+H)^+$] calcd for $C_{30}H_{29}FN_4O_6H^+$: 593.1865. HRMS-ES-EM: *m/z* = 615.1685 [$(M+Na)^+$] calcd for $C_{30}H_{29}FN_4O_6Na^+$: 615.1684. HPLC system **A**, method **A1** t_R =10.78 min (96%).

***N*⁴-(4-Fluoro-3-methylbenzyl)-*N*⁶-(4-hydroxybenzyl)pyrimidine-4,6-dicarboxamide (2c).** 6-((4-Fluoro-3-methylbenzyl)carbamoyl)pyrimidine-4-carboxylic acid (**10**, 26.0 mg, 0.091 mmol, 1.0 eq.) and 4-(aminomethyl)phenol (34.0 mg, 0.109 mmol, 1.2 eq.) were dissolved in a dichloromethane/acetonitrile mixture (1.2 mL, 3:1). Dry triethylamine (38 µL, 0.273 mmol, 3 eq.) and (benzotriazole-1-yloxy)tris(dimethylamino)phosphonium hexafluorophosphate (40 mg, 0.091 mmol, 1.0 eq.) were added and the reaction mixture was stirred for 12 h at room temperature. The solvent was removed under reduced pressure and the residue was purified by column chromatography (silica gel, CH/EA 1:1). The product was obtained as a colorless solid (38.2 mg, 0.065 mmol, 71%); mp 170°C with decomposition. ^1H NMR (250 MHz, $CDCl_3$) δ 9.16 (s, pyrimidineAr*H*, 1H), 8.92 (d, pyrimidineAr*H*, $^5J_{H,H}$ = 1.0 Hz 1H), 8.34 – 8.15 (m, N*H*, 2H), 7.20 (d, Ar*H*, $^3J_{H,H}$ = 8.5 Hz, 2H), 7.17 – 7.07 (m, Ar*H*, 2H), 6.96 (m, Ar*H*, 1H), 6.85 (d, $^3J_{H,H}$ = 8.5 Hz, 2H), 6.12 (br s, O*H*, 1H), 4.61 (t, $NHCH_2$, $^3J_{H,H}$ = 5.4 Hz, 4H), 2.25 (d, $ArCH_3$, $^4J_{H,F}$ = 1.7 Hz, 3H). ^{13}C NMR (63 MHz, $CDCl_3$) δ 161.93 (*C*ONH), 161.82 (*C*ONH), 160 85 (d, Ar*C*F, $^1J_{C,F}$ = 245.0 Hz), 158.81 (pyrimidineAr*C*), 158.61 (pyrimidineAr*C*), 156.62 (pyrimidineAr*C*H), 155.69 ($ArCOCH_3$), 132.73 (d, $ArCCH_2$, $^4J_{C,F}$ = 3.6 Hz), 131.13 (d, ArCH, $^3J_{C,F}$ = 5.3 Hz), 129.45 (Ar*C*H), 129.02 ($ArCCH_2$), 126.84 (d, Ar*C*H, $^3J_{C,F}$ = 8.2 Hz), 125.32 ($ArCCH_3$, $^2J_{C,F}$ = 17.5 Hz), 116.25 (pyrimidineAr*C*H), 115.70 (Ar*C*H), 115.25 (d, Ar*C*H, $^2J_{C,F}$ = 22.6 Hz), 43.31 ($NHCH_2$), 43.10 ($NHCH_2$), 14.50 (d, $ArCH_3$, $^2J_{C,F}$ = 3.5 Hz).^{19}F NMR (282 MHz, $CDCl_3$) δ -116.48 (m, 1F). HRMS-ES-EM: *m/z* = 395.1514 [$(M+H)^+$] calcd for $C_{21}H_{19}FN_4O_3H^+$: 395.1509. HRMS-ES-EM: *m/z* =

417.1326 [(M+Na)$^+$] calcd for $C_{21}H_{19}FN_4O_3Na^+$: 417.1333. HPLC system **A**, method **A1**: t_R =9.25 min (> 99%).

***N*^{4}-(4-Fluoro-3-methylbenzyl)-*N*^{6}-(4-methoxybenzyl)pyrimidine-4,6-dicarboxamide (2d).** To a solution of *N*^{4}-(4-fluoro-3-methylbenzyl)-*N*^{6}-(4-hydroxybenzyl)pyrimidine-4,6-dicarboxamide (**2c**, 28.0 mg, 0.071 mmol) in acetone (750 µL) potassium carbonate (29.0 mg, 0.213 mmol, 3 eq.) and dimethylsulfate (17 µL, 22.3 mg, 0.177 mmol, 2.5 eq.) were added and the reaction mixture was heated to reflux for 2 h. After cooling to room temperature, water (10 mL) was added and the aqueous layer was extracted with EA (3 x 5 mL). The combined organic phases were dried over magnesium sulfate and the solvent was removed under reduced pressure. The product was obtained as a colorless solid (28.0 mg, 0.068 mmol, 96%); mp 111 °C. ^{1}H NMR (250 MHz, $CDCl_3$) δ 9.08 (s, pyrimidineAr*H*, 1H), 8.86 (d, pyrimidineAr*H*, 1H), 8.24 – 7.97 (m, N*H*, 2H), 7.22 (d, Ar*H*, $^3J_{H,H}$ = 8.7 Hz, 2H), 7.19 (m, ArH, 1H), 7.17 – 7.00 (m, Ar*H*, 2H), 6.92 (m, Ar*H*, 1H), 6.81 (d, $^3J_{H,H}$ = 8.7 Hz, 2H), 4.54 (d, NHC*H*$_2$, $^3J_{H,H}$ = 5.8 Hz, 2H), 4.54 (d, NHC*H*$_2$, $^3J_{H,H}$ = 6.0 Hz, 2H), 3.73 (s, OC*H*$_3$, 3H), 2.19 (d, ArC*H*$_3$, $^4J_{H,F}$ = 1.7 Hz, 3H). ^{13}C NMR (63 MHz, $CDCl_3$) δ 161.83 (*C*ONH), 161.70 (*C*ONH), 160.84 (d, Ar*C*F, $^1J_{C,F}$ = 245.0 Hz), 159.22 (Ar*C*OCH$_3$), 158.86 (pyrimidineAr*C*), 158.68 (pyrimidineAr*C*), 156.57 (pyrimidineAr*C*H), 132.88 (d, Ar*C*CH$_2$, $^4J_{C,F}$ = 3.7 Hz), 131.12 (d, Ar*C*H, $^3J_{C,F}$ = 5.3 Hz), 129.44 (Ar*C*CH$_2$), 129.34 (Ar*C*H), 126.84 (d, Ar*C*H, $^3J_{C,F}$ = 8.2 Hz), 125.30 (Ar*C*CH$_3$, $^2J_{C,F}$ = 17.6 Hz), 116.27 (pyrimidineAr*C*H), 115.24 (d, Ar*C*H, $^2J_{C,F}$ = 22.5 Hz), 114.18 (Ar*C*H), 55.29 (O*C*H$_3$), 43.23 (NH*C*H$_2$), 43.05 (NH*C*H$_2$), 14.51 (d, Ar*C*H$_3$, $^2J_{C,F}$ = 3.6 Hz). ^{19}F NMR (282 MHz, $CDCl_3$) δ -116.67 (m, 1F). HRMS-ES-EM: *m/z* = 431.1494 [(M+Na)$^+$] calcd for $C_{22}H_{21}FN_4O_3Na^+$: 431.1490. HPLC system **A**, method **A3**: t_R =6.82 min (98%).

Radiochemistry. General Methods. [^{11}C]Methylation reactions were carried out on a custom-made radiosynthesizer consisting of two synthesis units, a HPLC unit and a formulation unit.[34] [^{11}C]CO_2 was produced by the $^{14}N(p,\alpha)^{11}C$ nuclear reaction performed on a 0.5% O_2/N_2 gas mixture using an IBA Cyclone 18/9 cyclotron (IBA, Louvain-la-Neuve, Belgium). Semi-prep isocratic HPLC was carried out with a Reprospher 100 C18-DE column (5 μm, 50 mm × 8 mm) using H_2O/CH_3CN/TFA (28:72:0.1, v/v/v) as the eluent at a flow rate of 5 mL · min^{-1}, a Jasco UV1575 UV detector (254 nm) and a custom-made radioactivity detector (HPLC system **C,** method **C1**). Analytical isocratic HPLC was carried out with a reverse-phase C18 Platinum column (5 μm, 250 mm × 4.6 mm; Eluent: H_2O/CH_3CN/TFA, 50:50:0.1, v/v/v; λ = 254 nm) as the eluent at a flow rate of 1 mL · min^{-1}, a Jasco UV-2075 Plus UV detector and a NaI radioactivity detector (Raytest, Straubenhardt, Germany) (HPLC system **D**, method **D1**). Analytical HPLC for metabolite analysis was performed with Dionex (Sunnyvale, CA, USA) UltiMate 3000 HPLC equipment with Chromeleon software (version 6.8) on a Phenomenex Gemini C18 column (5 μm, 250 mm × 10 mm) and a mixture of CH_3CN (A) and 0.1% TFA in water (B) as the eluent according to the following scheme (HPLC **E**, method **E1**): 0 min, 90% B at 0.25 mL·min^{-1}; 0.5 min, 90% B at 3.5 mL·min^{-1}; 9.0 min, 30% B at 3.5 mL·min^{-1}; 13.0 min, 30% B at 3.5 mL·min^{-1}; 14.0 min, 90% B at 3.5 mL·min^{-1}; and 15.0 min, 90% B at 0.25 mL·min^{-1}.

Remotely controlled radiofluorinations were carried out on a modified PET tracer radiosynthesizer (TRACERLab Fx_{FDG}, GE Healthcare). The recorded data were processed by the TRACERLab Fx software (GE Healthcare). Separation and purification of the radiosynthesized compounds were performed on the following semi-preparative radio-HPLC system **F** (λ=254 nm): K-500 and K-501 pump, K-2000 UV detector (Herbert Knauer GmbH), NaI(TI) Scintibloc 51 SP51 γ-detector (Crismatec) and a Phenomenex Gemini C18 column (5μ, 250 mm x 10 mm). The recorded data were processed by the GINA Star software

(Raytest Isotopenmessgeräte GmbH). Radiochemical purities and specific activities were determined using the analytical radio-HPLC system **A**. No-carrier-added aqueous [^{18}F]fluoride was produced on an RDS 111e cyclotron (CTI-Siemens) by irradiation of a 1.2 mL or 2.8 mL water target using 10 MeV proton beams on 97% enriched ^{18}O-water by the ^{18}O(p,n)^{18}F nuclear reaction.

Radiosynthesis of *N*^{4}-(4-fluoro-3-methylbenzyl)-*N*^{6}-(4-[^{11}C]methoxybenzyl)pyrimidine-4,6-dicarboxamide ([^{11}C]2d). [^{11}C]CO_2, carried by a helium stream (10 mL/min), was trapped in a solution of 0.1 M $LiAlH_4$ in THF (100 µL). THF was evaporated under helium flow by heating the reaction mixture to 130 °C. Subsequently, HI (225 µL, 60% in water) was added and the directly formed [^{11}C]CH_3I was distilled to the second reaction vial containing a solution of **2c** (1.0 mg, 2.5 µmol) and tetrabutylammonium hydroxide (1 µL, 1.5 µmol, 40% in water) in DMF (250 µL). The reaction mixture was heated for 2 min at 80 °C, diluted with the HPLC eluent (2 mL, H_2O/CH_3CN/TFA, 28:72:0.1, v/v/v) and purified by semi-prep-HPLC (**method C1**). The fraction containing [^{11}C]**2d** (t_R = 15.3 min) was collected, diluted with water (40 mL) and passed through a Waters Sep-Pak Plus tC18 cartridge, preconditioned with 10 mL of ethanol and 10 mL of water. The cartridge was washed with water (10 mL) and subsequently the product was eluted with ethanol (1 mL). The ethanol solution was diluted with 7.09 mM $NaHPO_4$ in saline, containing 1.6% of Polysorbate 80 (9 mL)and filtered over a Millex GV 0.2 µm filter. The product, **[^{11}C]2d**, was obtained in radiochemical yields of 36 – 50% (decay corrected, n = 4) from the end of radionuclide production with radiochemical purities > 98% and specific activities of 122 – 330 GBq/µmol in 29 ± 1 min. The identity of the product was confirmed with analytical HPLC by coinjection of **[^{11}C]2d** and the non-labeled compound **2d** (method **D1**, t_R = 7.7 min).

Radiosynthesis of *N*^{4}-(4-[^{18}F]fluoro-3-methylbenzyl)-*N*^{6}-(4-(2-fluoroethoxy)benzyl)pyrimidine-4,6-dicarboxamide ([^{18}F]2a). To recover the [^{18}O]water,

the batch of aqueous [^{18}F]fluoride was passed through an anion exchange resin (Sep-Pak Light Waters Accell Plus QMA cartridge, preconditioned with 5 mL 1 M K_2CO_3 and 10 mL water). [^{18}F]Fluoride was eluted from the resin with a mixture of 40 µL 1 M K_2CO_3, 200 µL water for injection, and 800 µL DNA-grade CH_3CN (ABX) containing 18 mg (0.48 mmol) Kryptofix 2.2.2 (K_{222}, ABX). Subsequently, the aqueous K(K_{222})[^{18}F]F solution was carefully evaporated to dryness *in vacuo* (2 min vacuum with helium stream, 1 min at 56°C without helium, then 8 min at 84°C without helium). Compound **2b** (3 mg, 5 µmol), dissolved in DNA-grade CH_3CN (500 µL) was added to the anhydrous K(K_{222})[^{18}F]F residue and the reaction mixture was heated at 110 °C for 15 min. The mixture was cooled to 40 °C and transferred to a 5 mL flask. The reactor was rinsed with hot ethanol (500 µL) and the combined organic phases were purified by gradient-radio-HPLC system **F**, method **F1** (flow = 5.5 mL/min, eluents: A: CH_3CN/TFA, 1000/1, B: H_2O/TFA, 1000/1; isocratic: A/B 45/55 (v/v); λ=254 nm; column: Phenomenex Gemini (C18, 5µ, 250 mm x 10 mm)). The product fraction of compound **[^{18}F]2a** (t_R = 13.1 min) was evaporated to dryness *in vacuo* and redissolved in 0.5 mL of 0.9% NaCl/EtOH (9/1 v/v). The target compound **[^{18}F]2a** was obtained in overall radiochemical yields of 21 ± 1% (decay corrected, based on cyclotron-derived [^{18}F]fluoride ions, n = 4) and radiochemical purities of > 98% after 75 ± 2 min from the end of radionuclide production. The determined specific activities were in the range of 18 – 35 GBq/μmol at the end of the synthesis.

Radiosynthesis of [^{68}Ga]gallium-2,2',2''-(10-(2-((2-(4-((6-((4-fluoro-3-methylbenzyl)carbamoyl)pyrimidine-4-carboxamido)methyl)phenoxy)ethyl)amino)-2-oxoethyl)-1,4,7,10-tetraazacyclododecane-1,4,7-triyl)acetic acid ([^{68}Ga]2i). Radiolabeling of the DOTA conjugate **2i** was performed on an iQS® Ga-68 Fluidic Labeling Module (ITG) with integrated ITG Ge-68/Ga-68 generator. Radiolabeling precursor **2i** (50 µg, 0.06 µmol) was dissolved in 1 mL of NH_4OAc buffer and heated at 105 °C for 5 min. Subsequently, the

generator was eluted with 0.05 N HCl (4 mL) and the eluate was added to the precursor solution. The labeling reaction was carried out in NH_4OAc/HCl buffer (pH 3.5 – 4) for 10 min at 105 °C. After HPLC separation (HPLC system **F**, method **F1**: flow = 5.5 mL/min, eluents: A: CH_3CN/TFA, 1000/1, B: H_2O/TFA, 1000/1; linear gradient from 10% to 60% A over 24 min; λ=254 nm; column: Phenomenex Gemini (C18, 5µ, 250 mm x 10 mm), t_R = 18.3 min), evaporation and formulation in phosphate buffered saline the product was obtained in radiochemical yields of 73 ± 5% (decay corrected, n = 4) with radiochemical purities > 99% in 74 ±1 min. The identity of the product was confirmed with analytical HPLC (method **A1**) by coinjection of **[^{68}Ga]2i** and the non-labeled compound **[Ga]2i** (t_R = 7.9 min).

***In vitro* enzyme inhibition assays (Table 1).** The inhibition potencies of pyrimidine dicarboxamides **2a, 2c-i**, **3a** and **4** against activated MMP-2, -8, -9, -13 and -14 were assayed using the synthetic fluorogenic substrate (7-methoxycoumarin-4-yl)acetyl-Pro- Leu-Gly-Leu-(3-(2,4-dinitrophenyl)-L-2,3-diaminopropionyl)Ala-Arg-NH_2 (R&D Systems) as described previously.[29] Briefly, MMP-2, -8, -9, -13 or -14 (each at 2 nM) and test compounds at varying concentrations (10 pM to 1 mM) in Tris (50 mM), pH 7.5, containing NaCl (0.2 M), $CaCl_2$ (5 mM), $ZnSO_4$ (20 µM), and 0.05% Brij 35 were preincubated at 37 °C for 30 min. An aliquot of substrate (10 µL of a 50 µM solution) was added to the enzyme−inhibitor mixture (90 µL), and the fluorescence changes were monitored using a TriStar2 Multimode Reader LB 942, (Berthold) with excitation and emission wavelengths of 340 and 405 nm, respectively. Reaction rates were measured from the initial 10 min and plotted as a function of inhibitor concentration. From the resulting inhibition curves, the IC_{50} values were calculated by nonlinear regression analysis using the Grace 5.1.8 software (Linux).

Determination of the partition coefficient (log *D* (exp.)). The lipophilicity of radioligands **[^{11}C]2d**, **[^{18}F]2a** and **[^{68}Ga]2i** were assessed by determination of the water-octanol partition coefficients following a published procedure.[35] In brief, approximately 20 kBq of **[^{11}C]2d**,

[^{18}F]2a and [^{68}Ga]**2i**, respectively, were mixed with equal amounts (0.5 mL) of PBS (pH 7.4) and 1-octanol and the resulting biphasic system was mixed vigorously for 1 min at rt. The tubes were centrifuged (3000 rpm, 2 min) and 400μL of the octanol phase were separated and again mixed with equal amounts (400 μL) of water. The resulting biphasic system was again mixed vigorously of 1 min at rt. After centrifugation (3000 rpm, 2 min) three samples of 100 μL of each layer were counted in a gamma counter (Wallac Wizard, Perkin-Elmer Life Science). The partition coefficient was determined by calculating the ratio cpm(octanol)/cpm(PBS) and expressed as log *D* (exp.) ($\log(cpm_{octanol}/cpm_{PBS})$). Two independent experiments were performed in triplicate and data were provided as mean values ± standard deviation.

***Ex vivo* biodistribution of [^{11}C]2d.** Healthy male balb/c mice (24 – 30 g) were injected with approximately 20 MBq **[^{11}C]2d** (at start of experiment) in the tail vein under isoflurane in 1-2% oxygen anaesthesia. The mice were sacrificed and dissected at 5, 15, 30 and 60 min post-injection (n = 4 per time point). Blood, heart, lungs, liver, kidneys, urine, brain, bone, muscle, intestine and gall bladder were collected, weighed and counted for radioactivity in a Wallac Universal Gamma Counter 1282 (PerkinElmer, Waltham, MA, USA). Biodistribution data were expressed as percentage injected dose per gram tissue (%ID/g).

Metabolism analysis of [^{11}C]2d. Four healthy male balb/c mice (28 – 31 g) were injected with 50 – 60 MBq of **[^{11}C]2d** in the tail vein under isoflurane anesthesia. Mice were sacrificed at 15 and 45 min p.i. (n = 2 per time point). Immediately, 0.5 mL of blood was collected via a heart puncture and collected in a heparin tube. The blood samples were centrifuged for 5 min at 4,000 rpm (Hettich universal 16, Depex, B. V., the Netherlands). Plasma was separated from the blood cells and 1 mL of the plasma was diluted with 2 mL of water and loaded onto a tC18 Sep-Pak (Waters, the Netherlands), preconditioned with 6 mL of methanol and 12 mL of water, respectively. The cartridge was washed with 3 mL of water to collect the polar

radioactive metabolites. Subsequently, the tC18 Sep-Pak cartridge was eluted with 2 mL of methanol and 1 mL of water to collect the mixture of apolar metabolites. The mixture of apolar metabolites was analyzed using HPLC method **E1** to determine the percentage of intact **[^{11}C]2d**.

***In vivo* biodistribution.** Adult C57/BL6 mice (male, 21-27 g) were anaesthetised by isoflurane in oxygen and one lateral tail vein was cannulated using a 27 G needle connected to 15 cm polyethylene catheter tubing. **[^{11}C]2d**, **[^{18}F]2a** or **[^{68}Ga]2i** (400 kBq/g bodyweight) was injected as a bolus (100 µL compound flushed with 100 µL saline) *via* the tail vein and subsequent PET scanning was performed.

Small animal PET scanning. PET experiments were carried out using a sub-millimeter high resolution (0.7 mm full width at half maximum) small animal scanner (32 module quadHIDAC, Oxford Positron Systems Ltd., Oxford, UK) with uniform spatial resolution (< 1 mm) over a large cylindrical field (165 mm diameter, 280 mm axial length).[36]

List-mode data were acquired for 120 min and reconstructed into dynamic time frames using an iterative reconstruction algorithm. Subsequently, the scanning bed was transferred to the computed tomography (CT) scanner (Inveon, Siemens Medical Solutions, U.S.) and a CT acquisition with a spatial resolution of 80 µm was performed for each mouse. Reconstructed image data sets were co-registered based on extrinsic markers attached to the multimodal scanning bed and the image analysis software (Inveon Research Workplace 3.0, Siemens Medical Solutions, USA). Three-dimensional volumes of interest (VOIs) were defined over the respective organs in CT data sets, transferred to the co-registered PET data and analyzed quantitatively. Regional uptake was calculated as percentage of injected dose by dividing counts per milliliter in the VOI by total counts in the mouse multiplied by 100 (%ID/mL).

Supporting Information

Experimental procedures and analytical data for the synthesis of compounds **2e** – **[Ga]2i**, **3a** – **b**, **4**, **5**, **6a** – **b**, **6e** – **f**, **6h**, **7a** – **b**, **7e** – **f**, **7h**, **11** – **13**, and NMR data of **5a** – **9a**. This material is available free of charge *via* the Internet at http://pub.acs.org.

AUTHOR INFORMATION

Corresponding Author

*Phone: +495731973551. Fax: +495731971819. Email: verena.hugenberg@gmx.de

Notes

The authors declare no competing financial interest.

ACKNOWLEDGEMENTS

The authors thank Christine Bätza, Stefanie Bouma, Claudia Essmann, Sven Fatum, Uta Funke, Wiebke Gottschlich, Sandra Höppner, Marlena Kattenbeck, Sarah Köster, Esther Kooijmann, Nina Kreienkamp, Carla F. M. Molthoff, Roman Priebe, and Katrin Reckmann, Marissa Rongen, Claudia Sewing and Marijke Stigter-van Walsum for technical support and the staff members of the Organic Chemistry Institute, University of Münster, Germany, for spectroscopic and analytical investigations. This work was supported by the Deutsche Forschungsgemeinschaft (DFG), International Isotope Society - Central European Devision (IIS-CED e. V.), Collaborative Research Center 656 (Molecular Cardiovascular Imaging Projects Z05 and C06) and the EU 7th Framework Programme (FP7/2007-2013) under grant agreement no. HEALTH-F2-2011-278850 (INMiND).

ABBREVIATIONS USED

CH, cyclohexane; EDC, *N*'-ethyl-*N*'-(3-dimethylaminopropyl)-carbodiimide hydrochloride; EA, ethyl acetate; EM, exact mass; FMT, fluorescence mediated tomography; FRI,

fluorescence reflectance imaging; GMP, Good Manufacturing Practice; HOBT, 1-hydroxy-benzotriazole; ICR, imprinting control region, K222, Kryptofix2.2.2; log *D*, log *P* at physiological pH (7.4), MMP, matrix metalloproteinase; MMPI, matrix metalloproteinase inhibitor; NMM: 4-methyl-morpholine; PEG, polyethylene glycol; PET, positron emission tomography; p.i., post injection; %ID, percentage injected dose; ROI, region of interest; SAR, structure-activity-relationship; SD, standard deviation; SPECT, single photon emission computed tomography; THP, tetrahydropyranyl; TIMP, tissue inhibitors of metalloproteinase: t_R, retention time.

---

[1] a) Matrix Metalloproteinases and TIMPs; Woessner, J. F.; Nagase, H.; Eds.; Oxford University Press: New York, **2000**; b) Whittaker, M.; Floyd, C. D.; Brown, P.; Gearing, A. J. Design and therapeutic application of metalloproteinase inhibitors. *Chem. Rev.* **1999**, *99*, 2735-2776.

[2] a) Fingleton, B. Matrix metalloproteinases: roles in cancer and metastasis. *Front. Biosci.* **2006**, *11*, 479-491. b) Kessenbrock, K.; Plaks, V.; Werb, Z. Matrix metalloproteinases: regulators of the tumor microenvironment. *Cell* **2010**, *141*, 52-67. c) Gialeli, C.; Theocharis, A. D.; Karamanos, N. K. Roles of matrix metalloproteinases in cancer progression and their pharmacological targeting. *FEBS J.* **2011**, *278*, 16-27.

[3] a) Galis, Z. S.; Khatri, J. J. Matrix metalloproteinases in vascular remodeling and antherogenesis: The good, the bad, and the ugly. *Circ. Res.* **2002**, *90*, 251-262. b) George S. J. Therapeutic potential of matrix metalloproteinase inhibitors in atherosclerosis. *Expert Opin. Invest. Drugs* **2000**, *9*, 993-1007.

[4] a) Okamoto, H.; Hoshi, D.; Kiire, A.; Yamanaka, H.; Kamatani, N. Molecular targets of rheumatoid arthritis. *Inflamm. Allergy Drug Targets* **2008**, *7*, 53-66. b) Troeberg, L.; Nagase, H. Proteases involved in cartilage matrix degradation in osteoarthritis. *Biochim. Biophys. Acta* **2012**, *1824*, 133-145.

[5] Honibald E. N.; Mathew, S.; Padmanaban, J.; Sundaram, E.; Ramamoorthy R. D. Perioceutics: Matrix metalloproteinase inhibitors as an adjunctive therapy for inflammatory periodontal disease. *J. Pharm. Bioallied Sci.* **2012**, *4*, (Suppl 2) 417-421.

[6] Muroski, M. E.; Roycik, M. D.; Newcomer, R. G.; Van den Steen, P. E.; Opdenakker, G.; Monroe, H. R.; Sahab, Z. J.; Sang, Q. X. Matrix metalloproteinase-9/gelatinase B is a putative therapeutic target of chronic obstructive pulmonary disease and multiple sclerosis. *Curr. Pharm. Biotechnol.* **2008**, *9*, 34-46.

[7] a) Brauer, P. R. MMPs-role in cardiovascular development and disease. *Front. Biosci.* **2006**, *11*, 447-478. b) Papazafiropoulou, A.; Tentolouris, N. Matrix metalloproteinases and cardiovascular diseases. *Hippokratia* **2009**, *13*, 76-82.

[8] Li, N. G.; Tang Y. P.; Duan, J. A.; Shi, Z. H. Matrix metalloproteinase inhibitors: a patent review (2011 – 2013). *Expert Opin. Ther. Pat.* **2014**, *24*, 1039-1052.

[9] a) Matusiak, N.; van Waarde, A.; Bischoff, R.; Oltenfreiter, R.; van de Wiele, C.; Dierckx, R. A.; Elsinga P. H. Probes for non invasive matrix metalloproteinase-targeted imaging with PET and SPECT. *Curr. Pharm. Des.* **2013**, *19*, 4647-4672.

[10] a) Cathcart, J. M.; Cao, J. MMP Inhibitors: Past, present and future. *Front. Biosci. (Landmark Ed.)* **2015**, *20*, 1164-1178. b) Vandenbroucke, R. E.; Libert, C. Is there new hope for therapeutic matrix metalloproteinase inhibition*? Nat. Rev. Drug Discov.* **2014**, *13*, 904-927.

[11] Li, J. J.; Johnson, A. R. Selective MMP-13 Inhibitors. *Med. Res. Rev.* **2011**, *31*, 863-894.

[12] De Savi, C.; Morley, A. D.; Ting, A.; Nash, I.; Karabelas, K.; Wood, C. M.; James, M.; Norris, S. J.; Karoutchi, G.; Rankine, N.; Hamlin, G.; MacFaul, P. A.; Ryan, D.; Baker, S. V.: Hargreaves, D.; Gerhardt, S. Selective non zinc binding inhibitors of MMP13. *Bioorg. Med. Chem. Lett.* **2011**, *21*, 4215-4219.

[13] Nara H.; Sato K.; Naito T.; Mototani, H, Oki, H,; Yamamoto Y.: Kuno H.; Santou, T.; Kanzaki, N.; Terauchi, J.; Uchikawa O.; Kori, M. Discovery of Novel, Highly Potent, and Selective Quinazolin-2-carboxamide-Based Matrix Metalloproteinase (MMP)-13 Inhibitors without a Zinc Bindng Group Using a Structure-Based Design Approach. *J. Med. Chem.* **2014**, 57, 8886-8902.

[14] Pendás, A. M.; Balbín, M.; Liano, E. Jiménez, M. G.; López-Otín, C. Structural Analysis and Promotor Characterization of the Human Collagenase-3 Gene (MMP-13). *Genomics*, **1997**, *40*, 222-233.

[15] Wernicke, D.; Seyfert, C.; Hinzmann, B.; Gromnica-Ihle, I. E.; Cloning of collagenase 3 from the synovial membrane and its expression in rheumatoid arthritis and osteoarthritis. *J. Rheumatol*. **1996**, *23*, 590-595.

[16] Knäuper, V.; Will, H.; López-Otín, C.; Smith, B.; Atkinson, S. J.; Stanton, H.; Hembry, R. M.; Murphy, G. Cellular mechanisms for human procollagenasee-3 (MMP-13) activation. Evidence that MT1-MMP (MMP-14) and gelatinase a (MMP-2) are able to generate active enzyme. *J. Biol. Chem.* **1996**, *271*, 17124-17131.

[17] Müller-Ladner, U.; Ospelt, C.; Gay, S.; Distler, O.; Pap, T. Development in the synovial biology field 2006. *Arthritis Res. Ther.* **2007**, *9*, 209.

[18] Nell, V. P. K.; Machold, K. P.; Stamm, T. A.; Eberl, G.; Heinzl, H.; Uffmann, M.; Smolen, J. S.; Steiner, G. Autoantibody profiling as early diagnostic and prognostic tool for rheumatoid arthritis. *Ann. Rheum.Dis.* **2005**, *64*, 1731-1736.

[19] Pendás, A. P.; Uría, J. A.; Jiménez, M. G.; Balbín, Freije, J. P.; López-Otín, C. An overview of collagenase-3 expression in malignant tumors and analysis of its potential value as a target in antitumor therapies. *Clin. Chim. Acta*, **2000**, *291*, 137-155.

[20] Vaalamo M.; Mattila, L.; Johansson N.; Kariniemi, A. L.; Karjalainen-Lindsberg, M. L.; Kähäri, V. M.; Saarialho-Kere U. Distinct population of stromal cells express collagenase-3

(MMP-13) and collagenase-1 (MMP-1) in chronic ulcers but not in normally healing wounds. *J. Invest. Dermatol.* **1997**, *109*, 96-101.

[21] Hernández, M.; Martínes, B.; Tejerina, J. M.; Valenzuela, M. A.; Gamonal, J. MMP-13 and TIMP-1 determinations in progressive chronic periodontitis. *J. Clin. Periodontol.* **2007**, *34*, 729-735.

[22] Sukhova, G. K.; Schönbeck, U.; Rabkin, E.; Schoen, F. J.; Poole, A. R.; Billinqhurst, R. C.; Libby, P. Evidence for increased collagenolysis by interstitial collagenase-1 and -3 in vulnerable human atheromatous plaques. *Circulation* **1999**, *99*, 2503-2509.

[23] Mao, D.; Lee, J. K.; VanVickle, S. J.; Thompson, R. W. Expression of collagenase-3 (MMP-13) in human abdominal aortic aneurysms and vascular smooth muscle cells in culture. *Biochem. Biophys. Res. Commun.* **1999**, *261*, 904-910.

[24] a) Engel, C. K.; Picard, B.; Schimanski, S.; Kirsch, R.; Habermann, J.; Klinger Q.; Schlotte V.; Weithmann K. U.; Wendt, K. U. Structural Basis for the Highly Selective Inhibition of MMP-13. *Chem. Biol.* **2005**, *12*, 181-189. b) Wassermann, Z. R. Making a turn in matrix metalloproteinase inhibitors. *Chem. Biol*. **2005**, *12*, 143-144.

[25] Klingler, O.; Kirsch, R.; Habermann, J.; Weithmann, K. U.; Engel, C.K.; Pirard, B. Selektive MMP-13 Inhibitoren. WO 2004/041788, 21.05.**2004**.

[26] Wagner, S.; Breyholz, H.-J.; Law, M.P.; Faust, A.; Höltke, C.; Schröer, S.; Haufe, G.; Levkau, B.; Schober, O.; Schäfers, M.; Kopka, K. Novel fluorinated derivatives of the broad-spectrum MMP inhibitors *N*-hydroxy-2(*R*)-{[(4-methoxyphenyl)sulfonyl](benzyl)- and (3-picolyl)-amino}-3-methyl-butanamide as potential tools for the molecular imaging of activated MMPs with PET. *J. Med. Chem*. **2007**, *50*, 5752-5764.

[27] Macleod, F.; Lang, S.; Murphy, J. A. The 2-(2-Azidoethyl)cycloalkanone strategy for bridged amides and medium-sized amine derivatives in the Aubé-Schmidt reaction. *Synlett* **2010**, 529-534.

[28] Glaser, M.; Årstad, E. Click labeling“ with 2-[^{18}F]fluoroethylazide for positron emission tomography. *Bioconjugate Chem.* **2007**, *18*, 989-993.

[29] Huang, W.; Meng, Q.; Suzuki, K.; Nagase, H.; Brew, K. Mutational study of the amino-terminal domain and human tissue inhibitor of metalloproteinases 1 (TIMP-1) locates an inhibitory region for matrix metallo proteinases. *J. Biol. Chem.* **1997**, *272*, 22086-22091.

[30] Rose, N. R.; Nq, S. S.; Mecinović, J.; Liénard B. M.; Bello S. H.; Sun, Z.; McDonough M. A.; Oppermann, U.; Schofield, C. J. Inhibitor scaffolds for 2-oxoglutarate-dependent histone lysine demethylases. *J. Med. Chem.* **2008**, *51*, 7053-7056.

[31] Macleod, F.; Lang, S.; Murphy, J. A. The 2-(2-Azidoethyl)cycloalkanone strategy for bridged amides and medium-sized amine derivatives in the Aubé-Schmidt reaction. *Synlett* **2010**, 529-534.

[32] Glaser, M.; Årstad, E. Click labeling“ with 2-[^{18}F]fluoroethylazide for positron emission tomography. *Bioconjugate Chem.* **2007**, *18*, 989-993.

[33] Wagner, S.; Breyholz, H.-J.; Law, M.P.; Faust, A.; Höltke, C.; Schröer, S.; Haufe, G.; Levkau, B.; Schober, O.; Schäfers, M.; Kopka, K. Novel fluorinated derivatives of the broad-spectrum MMP inhibitors *N*-hydroxy-2(*R*)-{[(4-methoxyphenyl)sulfonyl](benzyl)- and (3-picolyl)-amino}-3-methyl-butanamide as potential tools for the molecular imaging of activated MMPs with PET. *J. Med. Chem*. **2007**, *50*, 5752-5764.

[34] Windhorst, A.D.; Ter Linden, T.; De Nooij, A.; Keus, J.F.; Buijs, F.L.; Schollema, P.E.; van Rooij, L.F.; Herscheid, J.D.M. A complete, multipurpose, low cost, fully automated and GMP compliant radiosynthesis system. *J. Labelled. Compd. Radiopharm.* **2001**, *44*, S1052-S1054.

[35] Prante, O.; Hocke, C.; Löber, S.; Hübner, H.; Gmeiner, P.; Kuwert, T. Tissue distribution of radioiodinated FAUC113: assessment of a pyrazolo[1,5-*a*]pyridine-based dopamine D4 receptor radioligand candidate. *Nuklearmedizin* **2006**, *45*, 41-48.

[36] Schäfers, K.P.; Reader, A.J.; Kriens, M.; Knoess, C.; Schober, O.; Schäfers, M. Performance Evaluation of the 32-module quadHIDAC small animal PET scanner. *J. Nucl. Med*. **2005**, *46* (6), 996-1004.

TABLE OF CONTENTS GRAPHIC